JOURNAL OF MATERIALS RESEARCH AND TECHNOLOGY 2023;26:7829–7844

Available online at www.sciencedirect.com

jmr&t Journal of Materials Research and Technology

journal homepage: www.elsevier.com/locate/jmrt

A high corrosion-resistant waterborne epoxy resin coating improved by addition of multi-interface structured zinc phosphate particles

Hu Cai [a,1], *Xiteng Li* [a,1], *Yulin Zhang* [a], *Chao Yang* [a], *Suihan Cui* [a,**], *Liyuan Sheng* [b,c,*], *Daokui Xu* [d], *Ricky K.Y. Fu* [e], *Xiubo Tian* [a], *Paul K. Chu* [e], *Zhongzhen Wu* [a,***]

[a] *School of Advanced Materials, Peking University Shenzhen Graduate School, Shenzhen 518055, China*
[b] *Shenzhen Institute, Peking University, Shenzhen 518057, China*
[c] *PKU-HKUST ShenZhen-HongKong Institution, Shenzhen 518057, China*
[d] *Key Laboratory of Nuclear Materials and Safety Assessment, Institute of Metal Research, Chinese Academy of Sciences, Shenyang 110016, China*
[e] *Department of Physics, Department of Materials Science & Engineering, and Department of Biomedical Engineering, City University of Hong Kong, Tat Chee Avenue, Kowloon, Hong Kong, China*

ARTICLE INFO

Article history:
Received 21 July 2023
Accepted 12 September 2023
Available online 18 September 2023

Keywords:
3D multi-interface structured zinc phosphate
Epoxy-based waterborne paint
Corrosion resistance
Obstructing effect

ABSTRACT

In the present study, a three-dimensional multi-interface structured zinc phosphate particle with large specific surface area was prepared by regulating the zinc phosphate crystal growth process, which was applied to develop a waterborne epoxy resin coating with better corrosion resistance. The results reveal that the multi-interface structured zinc phosphate particles could well coalesce with epoxy resin. Compared with the waterborne coating doped with and without two-dimensional zinc phosphate sheets, the multi-interface structured zinc phosphate particles doped waterborne epoxy resin coating has highest corrosion potential, lowest corrosion current density and the highest low-frequency impedance, which indicates the obvious benefits of multi-interface structured zinc phosphate particles on corrosion resistance. Moreover, the electrochemical properties tests on the waterborne epoxy resin coatings immersed in salt solution for 3000 h demonstrate that the multi-interface structured zinc phosphate particles doped waterborne epoxy resin coating almost has no changes but the other waterborne epoxy resin coatings decrease obviously. The surface characterization on the corroded waterborne epoxy resin coatings reveal that the multi-interface structured zinc phosphate particles doped waterborne epoxy resin coating possesses the relative integrated surface, while the inner corrosion has occurred in other coatings. The waterborne epoxy resin coatings with different additives sprayed on Al alloy surface could obtain the adhesion strength between 6.21 and 6.81 MPa, and the multi-interface structured zinc phosphate particles doped waterborne epoxy resin coating possesses the maximum value. Even after the salt solution immersion for 3000 h, the multi-interface structured zinc phosphate particles doped waterborne epoxy resin coating still remains the adhesion strength above 6.21 MPa. Such excellent corrosion

* Corresponding author. Shenzhen Institute, Peking University, Shenzhen 518057, China.
** Corresponding author.
*** Corresponding author.
E-mail addresses: cuish@pku.edu.cn (S. Cui), lysheng@yeah.net (L. Sheng), wuzz@pku.edu.cn (Z. Wu).
[1] These authors contributed equally to this work.
https://doi.org/10.1016/j.jmrt.2023.09.109

resistance should be ascribed to the cooperation of strengthened physical inhibition effect, decreased polar channel and complexation reaction by multi-interface structured zinc phosphate particles.

1. Introduction

With the development of marine industry, the corrosion becomes an important challenge for the metal based structure components [1,2]. Though the conventional heavy-duty anti-corrosion coating could well protect the metal, however, its high requirement in content organic solvent would lead to great environment pollution [3,4]. Especially for the metal frame structure of offshore engineering, the conventional heavy-duty anti-corrosion coating also could influence the marine biological environment. Therefore, the waterborne coating with less pollution releasing has been paid more attention. Among them, the waterborne expoxy resin coating is the most potential one [5]. Now it is widely used in fields such as electronics [6], industry [7], and marine engineering due to their good mechanical properties [8], high chemical stability [9], strong metal adhesion [10], environmental friendliness [11], and low volatile organic compound (VOC) content [12]. Though the waterborne epoxy resin coating could obtain the ideal protecting effect in conventional environment, however, the large number of hydrophilic groups and surfactants inside would result in many polar channels, which is conducive to the penetration of corrosive media [13]. Corrosive media such as chloride ions can easily penetrate into the substrate and lead to inner corrosion, which destroys the coating by the formed corrosion product and decreases the service performance of the waterborne epoxy resin coating [14,15]. Therefore, how to extend the anti-corrosion service life of waterborne epoxy resin coating become a research focus for this kind of material.

Traditionally, the organic modification method is applied to control the high-density cross-linking reaction between functional groups for preparing coatings with high density and few pores, which can restrain the penetration rate of corrosive media [16]. For example, Wu et al. adjusted the precursor, catalyst, and additives, and designed a series of epoxy-sol–gel anti-corrosion coatings with high adhesion and good protective performance on aluminum surfaces by introducing cross-linking agents such as thiourea, mercaptan, and ene, which has improved the service life of the substrate obviously [17–19]. However, the efficacy of organic modification is limited by the environmental conditions such as high temperature, high humidity and sun exposure. Recently, researchers have shifted their focus to inorganic modifications such as graphene, MXene, boron nitride, and zinc phosphate. By introducing two-dimensional inorganic nanosheets as physical barriers, the "Labyrinth effect" can be realized to prolong the penetration path of corrosive media, which could be applied to improve the corrosion resistance. For example, Wang et al. [20] have modified the coatings with the graphene nanosheets because of its extremely low permeability, greatly improving the corrosion resistance property. However, due to its high conductivity of graphene, graphene nanosheets has to been oxidized or protected by the synthesized cyclodextrin-based supramolecular nano-containers which act as an "armor". Barsoum et al. [21–24] proposed to use MXene nanosheets with high permeability to replace graphene nanosheets, which also shows a good anti-corrosion effect. In addition, owing to the fact that the chemical stability of MXene material is poor, further functional group modifications are generally required. Hexagonal boron nitride (h-BN) nanosheets, which also present excellent insulating property (the conductivity is 10^{16}–10^{18} ohm cm^{-1} at room temperature) and chemical stability, can avoid the above problems when doped into the paints [25]. Nevertheless, h-BN nanosheets are generally synthesized by costly CVD techniques and h-BN nanosheets usually have poor compatibility with organic paints, which influences the adhesion strength with metal [26]. In comparison, zinc phosphate nanosheets can be chemically synthesized easily and possess good electrical insulation properties, which also displays strong anti-permeability performance (solubility product $K_{sp} = 9.1 \times 10^{-33}$) [27–29]. Moreover, it can form insoluble complex corrosion products with corrosive media through complexation reactions, which demonstrates a dual synergistic protection effect of physical shielding and chemical coupling to the substrate, therefore exhibiting significant advantages in epoxy coating modification [30]. However, it is difficult to achieve a completely ideal oriented arrangement of two-dimensional zinc phosphate sheet in the epoxy coating, which would inevitably influence the anti-corrosion properties, because of the decreasing of interface utilization rate. Then, it is important to regulate the structure and interface of zinc phosphate in epoxy coating to improve the anti-corrosion properties further.

Therefore, in the present research, the multi-interface structured zinc phosphate particles composed of two-dimensional sheet were fabricated and added in the waterborne epoxy resin paint. For comparison, the waterborne epoxy resin paint with two-dimensional zinc phosphate sheet were prepared simultaneously. These paints were sprayed on Al alloy specimens and the electrochemical properties and long-term immersion corrosion tests have been performed to investigate the effect of zinc phosphate structure. The adhesion strength before and after immersion corrosion was tested to evaluate its application prospect.

2. Material and methods

2.1. Materials

The LY12 Al alloy (30 mm × 30 mm × 1 mm) were purchased from Dongguan Guanyue Metal Materials Co., Ltd. (Dongguan, China), analytical grade chemical reagents including

ammonium carbonate, ammonia water (25 wt%), and absolute ethanol were bought from Guangdong Xilong Chemical Co., Ltd. (Shantou, China), and analytical grade Acetone, polyethylene glycol −2000, phosphoric acid, and two-dimensional sheet-like zinc phosphate were provided by Aladdin Biochemical Technology Co., Ltd. (Shanghai, China). Zinc oxide particles with diameters of 50–100 nm were purchased from Sinopharm Chemical Reagents Co., Ltd. (Shanghai, China). Bisphenol A epoxy resin MU-618, polyamine modified epoxy curing agent CU-600, and all other reagents were obtained from Hangzhou Qingci New Materials Co., Ltd. 1500 mesh metallographic sandpapers were purchased from 3 M China Co., Ltd. (Shanghai, China). All the reagents were used without treatment.

2.2. Preparation of multi-interface structured zinc phosphate particles

15.00 g of ammonia water and 3.75 g of ammonium carbonate were added to 20.00 g of deionized water and stirred at a rate of 300 r/min for 15 min until completely dissolution in the alkaline solution. 1.00 g of zinc oxide and 0.40 g of polyethylene glycol −2000 were then introduced and stirred until complete dissolution. The Zn-containing solution was dispersed ultrasonically for 50 min and placed in a 60 °C water bath for 10 min. The 2.00 g/20.0 mL phosphoric acid/alcohol solution was dripped at a rate of 0.6 mL/min into the solution to start the precursor reaction. After titration, the solution containing zinc phosphate was stirred at a rate of 400 r/min for 40 min, left to stand for 10 min, washed with deionized water 5 times, and then filtered to obtain the solid powder which was dried in an oven at 90 °C for 12 h to obtain the multi-interface structured zinc phosphate particles.

2.3. Preparation of waterborne epoxy resin paints

The Al alloy substrate was polished with 1500 mesh metallographic sandpaper, ultrasonically cleaned with deionized water, absolute ethanol, and acetone for 30 min successively, and dried for later use. 1.00 g of the 3D multi-interface zinc phosphate particles were added to 10.00 g of bisphenol A epoxy resin paint (MU-618) and stirred for 60 min at a rate of 800 r/min. 5.00 g of the polyamine modified epoxy curing agent (CU-600) were introduced and stirred for 30 min to obtain paints uniformly doped with multi-interface structured zinc phosphate particles. Paints with different doping concentrations were prepared by changing the amount of zinc phosphate. The paints were uniformly sprayed on the metal substrate by a spray gun at a pressure of 0.6 MPa and cured at room temperature for 6 h. After further curing in an oven at 90 °C for 2 h, the paint coated with multi-interface structured zinc phosphate particles was obtained and designated as Epoxy@ZPNF. The pure resin paint and paint modified by two-dimensional zinc phosphate sheet were prepared by the same process as controls and labeled Epoxy and Epoxy@ZPNS.

2.4. Characterization

Field-emission scanning electron microscopy (FESEM, Carl Zeiss, SUPRA® 55, GER) was used to observe the morphology of multi-interface structured zinc phosphate particle, two-dimensional zinc phosphate sheet, and doped paints before and after corrosion. The chemical composition of the paints was determined by energy-dispersive X-ray spectroscopy (EDS, Oxford, X-Max20, GB). X-ray diffraction (XRD, Bruker, D8 Advance, GER) was adopted to analyze the phase constitutent of the multi-interface structured zinc phosphate particles and two-dimensional zinc phosphate sheet. The XRD scanning rate was 5°/min and step length of 0.05 s, with 2θ range of 10°–90° and a Cu target ($\lambda = 0.15418$ nm). High-resolution transmission electron microscopy (TEM, JEM-3200FS, Japan) was conducted to study the crystal structure and phase composition. The chemical composition and bonding of the multi-interface structured zinc phosphate particles and two-dimensional zinc phosphate sheet were determined by X-ray photoelectron spectroscopy (XPS, Thermo Fisher, ESCALAB 250X, USA) referenced to the C 1s peak (284.8 eV). The energy spectra of different elements were fit by an analysis software (Avantage 5.978, USA). The chemical bonds and functional groups of different zinc phosphate doped paints were determined by FTIR (PerkinElmer, USA). A 3D laser confocal microscope (LCSM, VK-X200 series, Keyence Corporation of America, USA) was employed to analyze the surface profile of the paint and a tensile machine (ZQ-990LA, ZHIQU, China) was used to determine the adhesion strength between the paint and Al alloy substrate.

2.5. Electrochemical and salt-solution immersion tests

The electrochemical properties of the paints coated Al alloy specimens were determined in 3.5 wt% NaCl using an electrochemical workstation (NPROBE/EPC42, Zahner, GER) with a three-electrode configuration at room temperature (25 °C). An Al alloy sample with an exposed area of 2.4 cm^2 was the working electrode and saturated calomel (SCE) was the reference electrode. The open circuit potential (OCP) was determined in the NaCl solution to stabilize the system. EIS was carried out with a sine signal of 10 mV from 100 kHz to 0.1 Hz. The impedance data were fitted and analyzed by the ZsimpWin software. The Al alloy were fitted by the R (QR) (QR) equivalent circuit, while the samples coated with paints were fitted by the R (Q (R (QR)) equivalent circuit. The Tafel test was carried out at scanning rate of 1 mV/s and the corrosion potential (E_{corr}) and corrosion current density (i_{corr}) of the sample were obtained by Tafel extrapolation. Specifically, the value at the intersection of the anode and cathode curves is the corrosion potential, while the current density at the intersection of the curve tangents is the corrosion current density. The immersion experiment was performed in a 200.0 mL beaker with the sample immersed in 150.0 mL of the NaCl solution (5 wt%) at room temperature for 3000 h (solution changed every 48 h). After immersion, the samples were washed with water and ethanol and then dried prior to the Tafel and EIS electrochemical tests.

3. Results and discussion

3.1. Material characterization

The microstructure observations on commercial two-dimensional zinc phosphate sheets show the irregular

lamellar morphology. The length or width of the zinc phosphate sheets are about 10–50 μm and their thickness is about 200–500 nm, as shown in Fig. 1(a) and (d). The XRD pattern shows that the zinc phosphate sheet is composed of $Zn_3(PO_4)_2{\cdot}4H_2O$ and $Zn_3(PO_4)_2{\cdot}2H_2O$, as presented in Fig. 1(b). The diffraction peaks strength indicates the $Zn_3(PO_4)_2{\cdot}4H_2O$ has high ratio. Moreover, the zinc phosphate sheets demonstrate high-ratio of low index crystallographic plane. Fig. 1(c) and S1(a) shows the presence of a large number of hydroxyl groups in the zinc phosphate sheet according to XPS and FT-IR analyses. The peak intensity of O–H in O1s and the vibration peak belonging to O–H at 3100-3500 cm^{-1} both indicate the existence of water in the form of crystalline water in the zinc phosphate sheet. The energy spectra of Zn2p and P2p in the full spectrum are correspond to Zn^{2+} and PO_4^{3-}, respectively (Figs. S1(d) and S1(e)). HRTEM observations on the zinc phosphate sheet reveal that the nano-size $Zn_3(PO_4)_2{\cdot}4H_2O$ phases have random crystallographic orientation, as shown in Fig. 1(e) and (f). Moreover, the amorphous structure could be observed along $Zn_3(PO_4)_2{\cdot}4H_2O$ phases junction, which implies this unstable phase would be apt to react with corrosion medium [31]. Fig. 1(g) shows the elemental mapping analyses on the zinc phosphate sheet, and the inhomogeneous element distribution can be seen. The simultaneous segregation of Zn and P indicates the different crystalline water ratio in different phases.

Fig. 2(a) shows that the synthesized zinc phosphate particles have a flower-like structure and contain many two-dimensional lamellae, which could designated as multi-interface structured zinc phosphate particle. The dimension analyses reveal the diameter of whole zinc phosphate particle is about 2–5 μm, while the thickness of the two-dimensional lamella is about 10–50 nm. Compared with the commercial zinc phosphate sheet, the synthesized zinc phosphate particle is much smaller and has higher specific surface area. The XRD analyses reveal that the synthesized zinc phosphate particles are mainly composed of $Zn_3(PO_4)_2{\cdot}4H_2O$ phase with highly preferred (111) and (241) crystallographic plane, as shown in

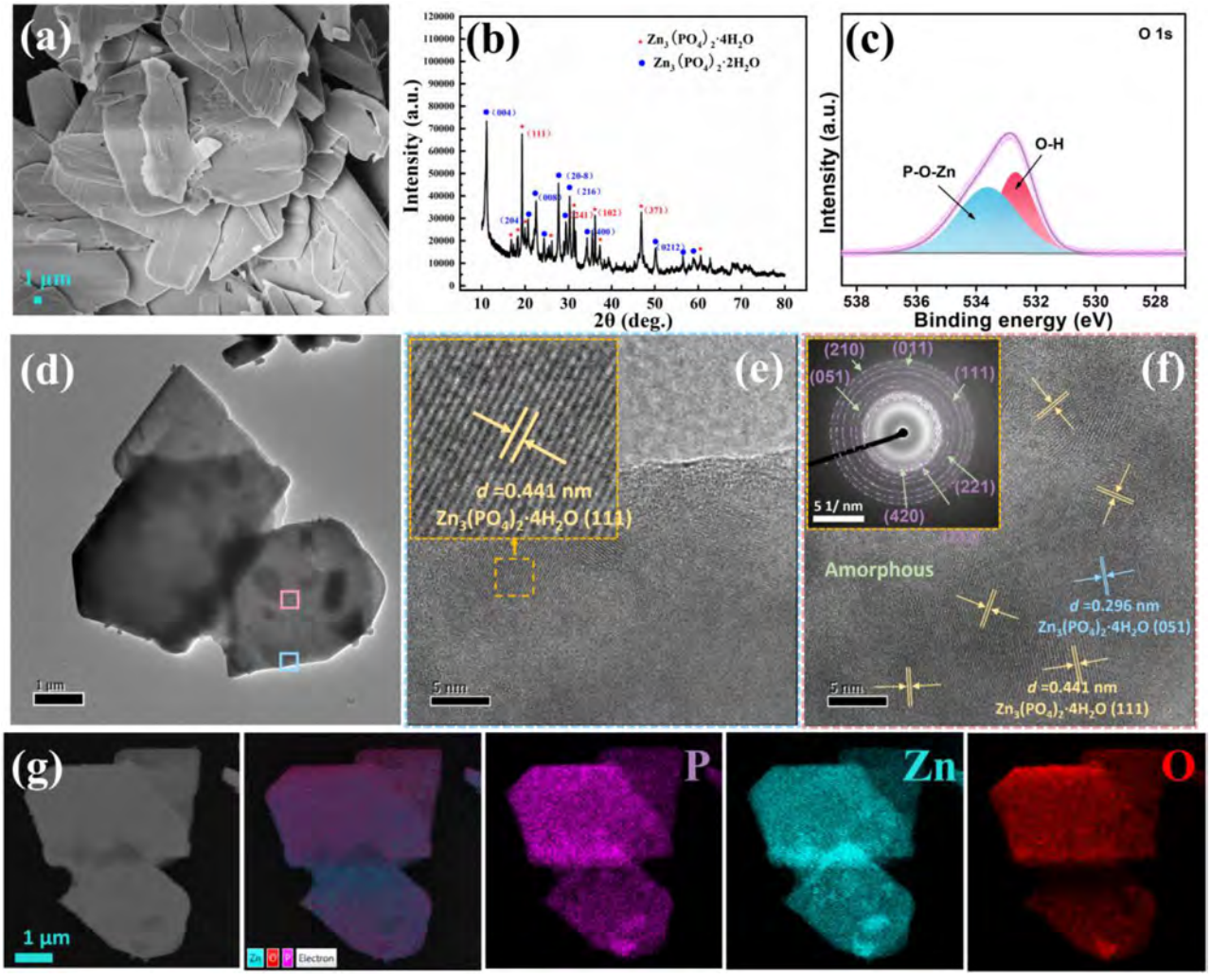

Fig. 1 – Characterization on the two-dimensional zinc phosphate sheet: (a) SEM observation showing the morphology, (b) XRD analysis on the phase and crystal orientation, (c) XPS spectra showing the bonding features; (d) TEM observation showing the multiphase feature, (e) HRTREM image on the $Zn_3(PO_4)_2{\cdot}4H_2O$ phase (Inset image showing the atomic line lattice), (f) HRTEM image showing the compound of amorphous and zinc phosphate (Inset image showing the SAED pattern), (g) Elemental mapping of the zinc phosphate sheet in (d).

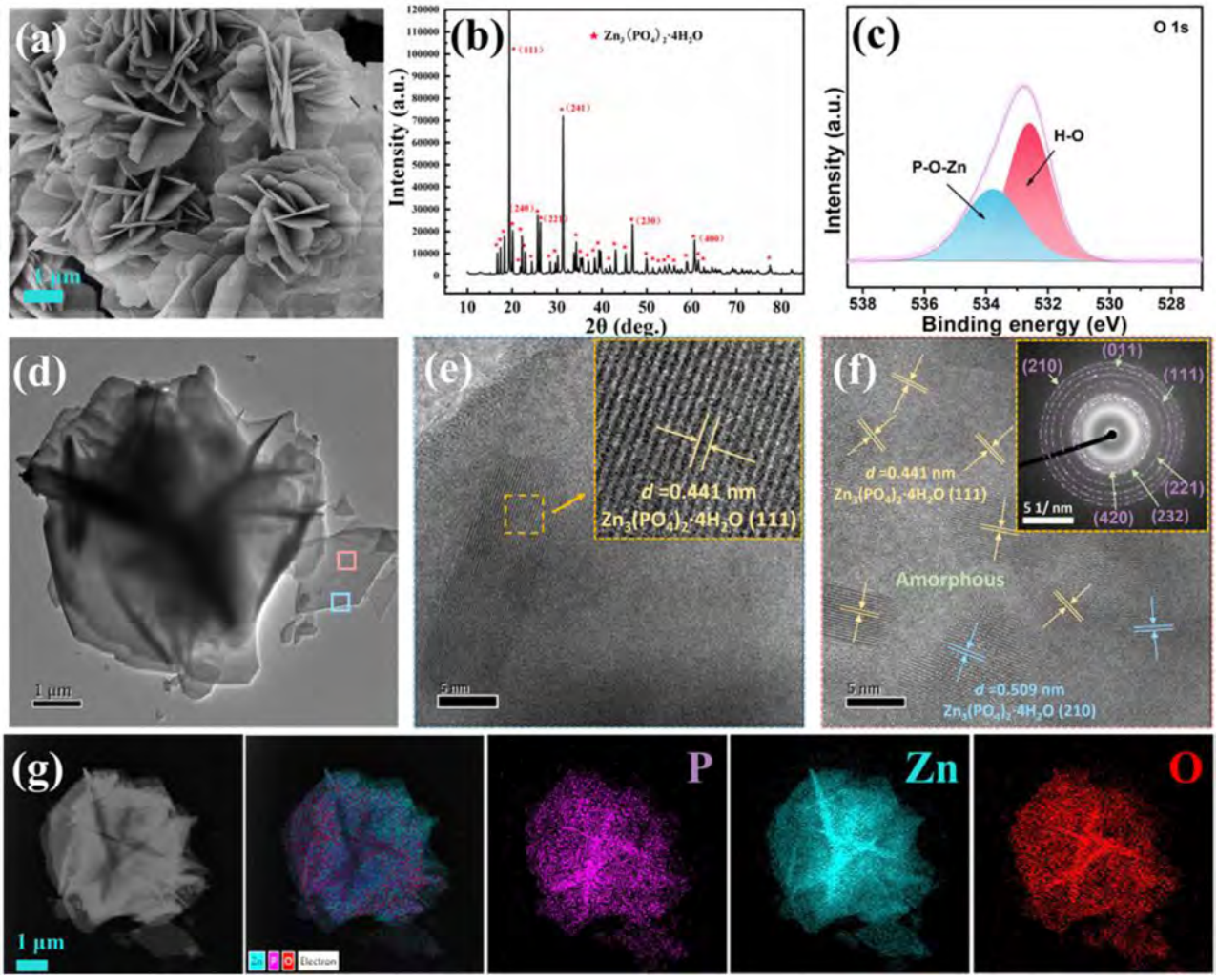

Fig. 2 – Characterization on the multi-interface structured zinc phosphate particles: (a) SEM observation showing the morphology, (b) XRD analysis on the phase and crystal orientation, (c) XPS spectra showing the bonding features, (d) TEM observation showing the stereostructure feature, (e) HRTREM image on the $Zn_3(PO_4)_2{\cdot}4H_2O$ phase (Inset image showing the atomic line lattice), (f) HRTEM image showing the compound of amorphous and zinc phosphate (Inset image showing the SAED pattern), (g) Elemental mapping of the multi-interface structured zinc phosphate particle in (d).

Fig. 2(b). Fig. 2(c) shows that the peak fitting of the XPS spectrum of the multi-interface structured zinc phosphate particles. The O–H peak intensity in the O1s spectrum and the 3100-3500 cm^{-1} position of the O–H vibration peak were both significantly higher than those of commercial two-dimensional zinc phosphate sheet. The FT-IR spectrum shows similar result (S1(b)). Combined with the XRD results, it can be concluded that the O–H bond mainly comes from crystal water, and the content of crystal water in the multi-interface structured zinc phosphate particle is significantly higher than that in commercial two-dimensional zinc phosphate sheet. This can be attributed to the fact that zinc phosphate crystallizes and grows in a low-temperature aqueous environment, which can absorb more crystal water. Meanwhile, the spatial confinement effect of the tiny pores in the three-dimensional multi-interface structure can lock the crystal water [32]. The XPS full spectrum and the enlarged spectra of Zn2p and P2p of the multi-interface structured zinc phosphate particles are presented in Fig. S1(f)-S1(h). The spectral results confirm that the elements and hybrid forms contained in the multi-interface structured zinc phosphate particles are basically the same as those of commercial two-dimensional zinc phosphate sheet. The multi-interface structured zinc phosphate particle contains core frame and branch lamella was analyzed by TEM, as displayed in Fig. 2(d). The thin branch lamellae are inlaid with core frame, ensuring the structural stability. Fig. 2(e) and (f) shows the thin lamella demonstrate that the $Zn_3(PO_4)_2{\cdot}4H_2O$ phases prefer to grow along (111) crystallographic plane. Moreover, the ratio of amorphous in the zinc phosphate is increased, which indicates the high chemical activity of as synthesized multi-interface structured zinc phosphate particles. Combining with the high specific surface area, it can be deduced that the multi-interface structured would possess better corrosion medium inhabition effect.

The waterborne epoxy resin paints with additions of two-dimensional zinc phosphate sheet and multi-interface structured zinc phosphate particles were sprayed on the Al alloy

substrate. For comparison, the pure waterborne epoxy resin paint was also sprayed on the Al alloy substrate. The as-sprayed coatings were cured and their surface morphology are given in Fig. S2. It can be found that the addition of zinc phosphate could promote the flatting of the waterborne epoxy resin coating, especially the coating with multi-interface structured zinc phosphate particles. Such a phenomena should be ascribed partly to the catalytic effect of the multi-amine-modified epoxy curing agent CU-600, which could easily opens the adjacent epoxy bonds and form a three-dimensional cross-linked network of N–C bonds and a large number of hydroxyl groups. The hydroxyl groups of resin can coordinate with the hydroxyl groups of zinc phosphate to form intermolecular hydrogen bonds, which could achieve well matched interface and relieve the internal stress. Therefore, the coatings with zinc phosphate addition possesses the better surface morphology.

Fig. 3 shows the cross-sectional morphology of the waterborne epoxy resin coatings, which is relative densified and have good adhesive interface. The SEM observations on the waterborne epoxy resin coating exhibit that there are micropores with size of 100–500 nm, as shown in Fig. 3(a)–(c). The two-dimensional zinc phosphate sheet doped waterborne epoxy resin coating demonstrate that the two-dimensional zinc phosphate sheets distribute with different posture with most zinc phosphate sheets paralleling to the coating surface, as listed in Fig. 3(d)–(f). The micropores still could be observed in the cross-section of two-dimensional zinc phosphate sheet doped waterborne epoxy resin coating. Such morphology of zinc phosphate sheets could take full use of their interface to restrain the infiltration of corrosion medium. As shown in Fig. 3(g)–(i), the multi-interface structured zinc phosphate particles doped waterborne epoxy resin coating demonstrate that these particles are well inlaid in the coating with matched interface. That indicates that hydrogen bonds significantly enhance the wettability and binding between zinc phosphate and waterborne epoxy resin coating.

Fig. 4(a) shows the elemental distributions of C and O in the cross-section of the waterborne epoxy resin coating reveal. There are many micropores in the cross-section, which would prefer to form the polar channels during the service of the coating. The addition of zinc phosphate sheets could produce

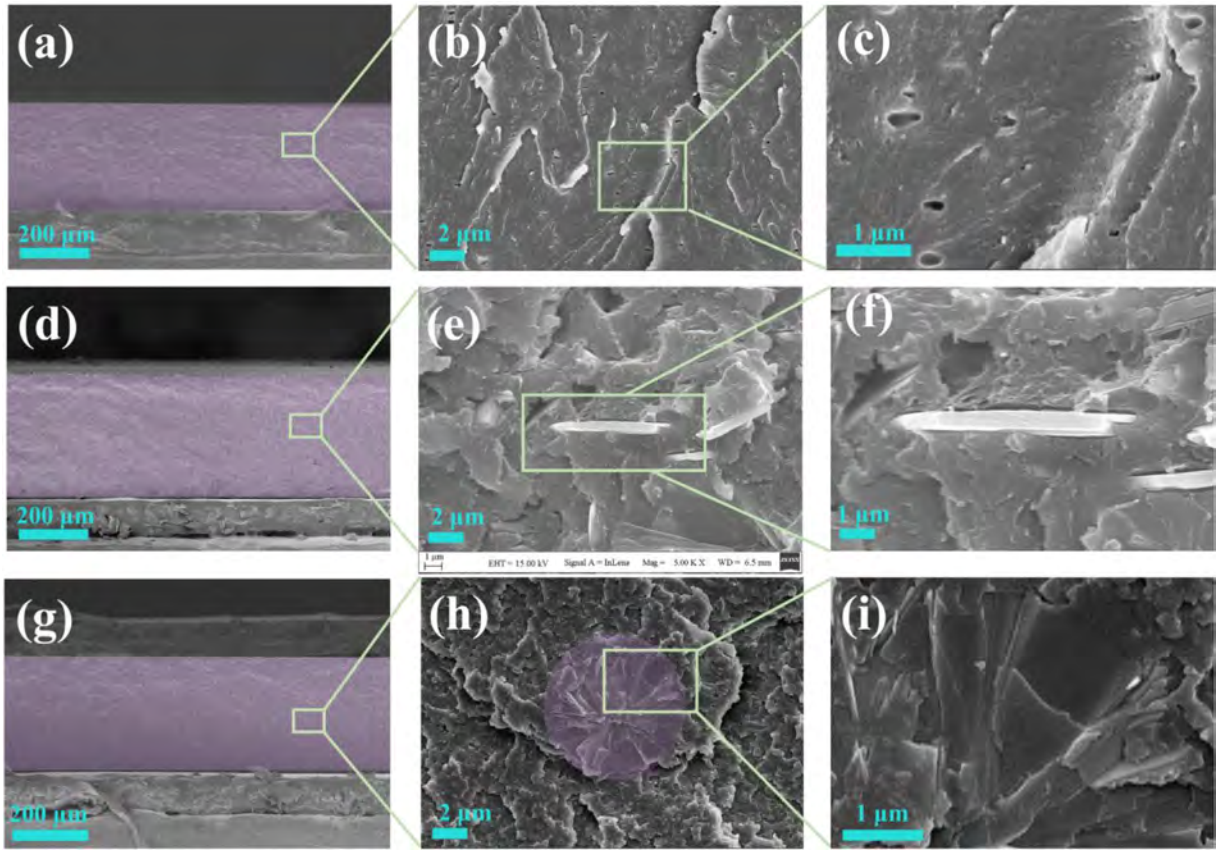

Fig. 3 – SEM observations on the cross-section of the waterborne epoxy resin coatings: (a) Cross-sectional morphology of waterborne epoxy resin coating, (b) Magnified SEM image showing the micropores in (a), (c) SEM image showing the micropores with different size in (b), (d) Cross-sectional morphology of waterborne epoxy resin coating doped with two-dimensional zinc phosphate sheet; (e) Magnified SEM image showing the distribution of zinc phosphate sheet in (d), (f) SEM image showing the interface of zinc phosphate sheet in (e); (g) Cross-sectional morphology of waterborne epoxy resin coating doped with multi-interface structured zinc phosphate particles, (h) Magnified SEM image showing the inlaid multi-interface structured zinc phosphate particle in (g), (i) SEM image showing the interface of multi-interface structured zinc phosphate particle in (h).

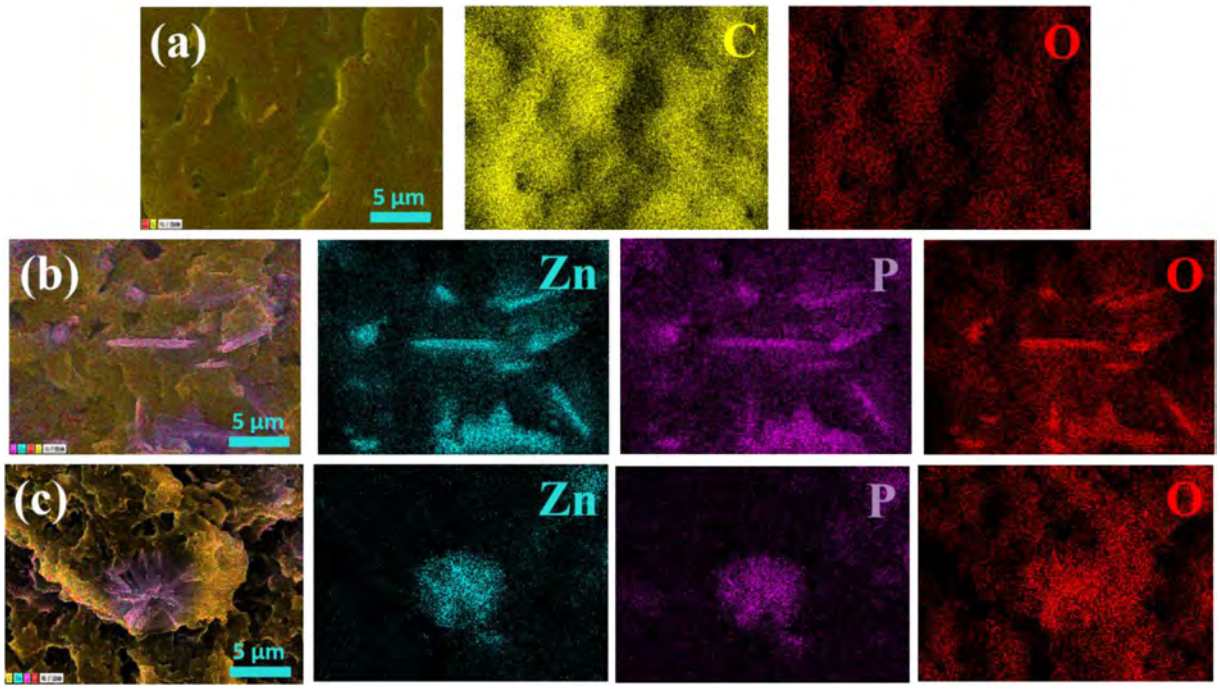

Fig. 4 – Elemental mapping distribution on the cross-section of the waterborne epoxy resin coatings: (a) Waterborne epoxy resin coating, (b) Two-dimensional zinc phosphate sheets doped waterborne epoxy resin coating, (c) Multi-interface structured zinc phosphate particles doped waterborne epoxy resin coating.

the discontinuous shield, as shown in Fig. 4(b). Moreover, the diffusion of Zn and P in the coating matrix also indicate the interaction between zinc phosphate and epoxy resin during curing. The multi-interface structured zinc phosphate particles doped waterborne epoxy resin coating demonstrates less diffusion of Zn and P, which indicates the relative stability of synthesize zinc phosphate, as presented in Fig. 4(c). The FT-IR tests results indicate that all coatings exhibit O–H vibration absorption peaks in the 3100-3500 cm^{-1} range, but the multi-interface structured zinc phosphate particles doped coating has the O–H peak intensity, which means more hydroxyl groups have formed by the zinc phosphate, as shown in Fig. S3. Additionally, the two-dimensional zinc phosphate sheets doped coating also demonstrates the relative strong O–H vibration absorption peaks in the same range. The increased hydroxyl groups would strengthen the bonding between the zinc phosphates and epoxy resin, which helps to block the polar channels and contributes to the corrosion resistance.

3.2. *Electrochemical performance*

Fig. 5 shows the electrochemical properties of different kinds of coating specimens. After optimization of the zinc phosphate concentration and coating thickness (Figs. S4–S6 and Tables S1–S6), the Tafel curves of the specimens with the best performance are shown in Fig. 5(a). Compared to the aluminum alloy substrate, the corrosion potential of the waterborne epoxy resin coating, the two-dimensional zinc phosphate sheets doped coating, and the multi-interface structured zinc phosphate particles doped coating increases from −1.50 V to −0.98 V, −0.87 V, and −0.73 V, respectively. The corresponding corrosion current density decreases from 7.60×10^{-4} A·cm^{-2} to 5.62×10^{-6} A·cm^{-2}, 6.11×10^{-7} A·cm^{-2}, and 3.98×10^{-9} A/cm^2, respectively (Table 1). Compared with the waterborne epoxy resin coating, the zinc phosphates addition could improve the corrosion resistance significantly, especially the zinc phosphates particles with multi-interface structure.

In the Nyquist spectrum, all coating specimens show significant capacitance behavior, and the capacitance loop of the multi-interface structured zinc phosphate particles doped coatings has the largest diameter, indicating the largest electrochemical impedance, as depicted in Fig. 5(b). Further analysis of the Bode-impedance data shows that the impedance modulus of the waterborne epoxy resin coating is close to 2 orders of magnitude higher than that of the Al alloy substrate in the low-frequency region, increasing from 5.28×10^3 ohm cm^2 to 9.73×10^4 ohm cm^2. The impedance of the two-dimensional zinc phosphate sheets doped coating further increases to 3.29×10^5 ohm cm^2, while the impedance of the multi-interface structured zinc phosphate particles doped coating increases to a maximum of 3.74×10^7 ohm cm^2, as shown in Fig. 5(c). Fig. 5(d) shows the Bode-phase data of reveals that the Al alloy and all coatings specimens. It can be seen that the phase angle of the multi-interface structured zinc phosphate particles doped coating has the highest value in the high-frequency region, indicating the best capacitance and the least solution penetration. In the low-frequency region, the phase angle values of all coatings are much lower than that of the Al alloy, indicating that the coatings have a good current cutoff effect. That may be attributed to the well bonding of multi-interface structured zinc phosphate particles with the epoxy resin coating. In the early stage of

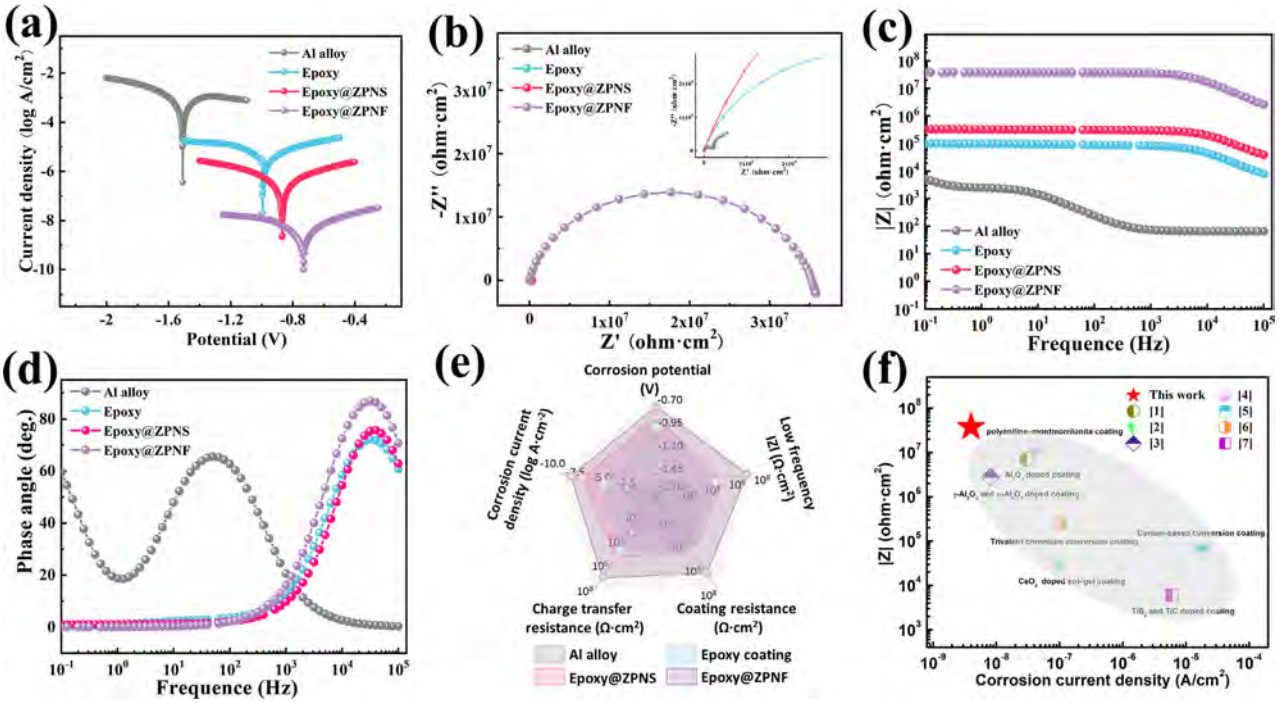

Fig. 5 – Comparison of the electrochemical properties of the Al alloy and its specimens coated by waterborne epoxy resin coating (Epoxy), waterborne epoxy resin coating doped with two-dimensional zinc phosphate sheet (Epoxy@ZPNS) and waterborne epoxy resin coating doped with multi-interface structured zinc phosphate particles (Epoxy@ZPNF): (a) Tafel curves, (b) Nyquist data, (c) Bode-absolute data, (d) Bode-phase data, (e) Electrochemical performance and (f) Comparison with materials in the literature.

corrosion, the participation of highly impermeable zinc phosphate could improve the corrosion resistance by shielding effect.

In addition, according to the time constants of each specimen in the Bode-phase data, two equivalent circuit (EC) models, R (QR) (QR) and R (Q (R (QR))) [33], were used to fit the Al alloy and all coatings to obtain the corresponding electronic component values (Table 2). The time constant at high frequency corresponds to the coating, and the time constant at low frequency corresponds to the electric double layer. The five key electrochemical data of each specimen, including corrosion potential, corrosion current density, low-frequency impedance value, interface charge transfer resistance, and coating resistance, were compared in a pentagon coordinate system, as shown in Fig. 5(e). It is evident that the multi-interface structured zinc phosphate particles doped coating exhibits the largest pentagon area, indicating its superior anti-corrosion performance. In some extent, the *CPE* could reflect the high-frequency impedance of the coating. The smaller the *CPE*, the better the high-frequency capacitance and the larger the high-frequency impedance. The higher the low-frequency impedance value, the better the low-frequency resistance, and the stronger the coating's ability to resist the penetration of corrosive media. Compared to the Al alloy substrate, the CPE_c of the waterborne epoxy resin coating, the two-dimensional zinc phosphate sheets doped coating, and the multi-interface structured zinc phosphate particles doped coating decrease from 3.223×10^{-4} $ohm^{-1}\cdot cm^{-2}\cdot s^n$ to 7.531×10^{-10} $ohm^{-1}\cdot cm^{-2}\cdot s^n$, 8.067×10^{-11} $ohm^{-1}\cdot cm^{-2}\cdot s^n$, and 7.564×10^{-13} $ohm^{-1}\cdot cm^{-2}\cdot s^n$, respectively. The corresponding CPE_{dl} exhibits a same trend, decreasing from 6.385×10^{-6} $ohm^{-1}\cdot cm^{-2}\cdot s^n$ to 4.788×10^{-6} $ohm^{-1}\cdot cm^{-2}\cdot s^n$, 1.023×10^{-9} $ohm^{-1}\cdot cm^{-2}\cdot s^n$, and 2.146×10^{-13} $ohm^{-1}\cdot cm^{-2}\cdot s^n$, respectively (Table 2). Meanwhile, the multi-interface structured zinc phosphate particles doped coating exhibits the maximum low-frequency impedance value of 3.74×10^7 ohm cm^2, and the coating resistance R_c and interfacial charge transfer resistance R_{ct} both remaine above 10^7 ohm cm^2. The highest values of high-frequency capacitance and low-frequency resistance of the multi-interface structured zinc phosphate particles doped coating implies its excellent corrosion resistance performance. Compared with the electrochemical performance of waterborne coatings in recent researches, the present multi-interface structured zinc phosphate particles doped coating has better corrosion resistance with the

Table 1 – Corrosion potentials and corrosion current densities of the Al alloy and its specimens coated by waterborne epoxy resin coating (Epoxy), waterborne epoxy resin coating doped with two-dimensional zinc phosphate sheet (Epoxy@ZPNS) and waterborne epoxy resin coating doped with multi-interface structured zinc phosphate particles (Epoxy@ZPNF).

Sample	E_{corr} (V)	i_{corr} ($A\cdot cm^{-2}$)
Al alloy	−1.50	7.60×10^{-4}
Epoxy	−0.98	5.62×10^{-6}
Epoxy@ZPNS	−0.87	6.11×10^{-7}
Epoxy@ZPNF	−0.73	3.98×10^{-9}

Table 2 – EIS fitting data of the Al alloy and its specimens coated by waterborne epoxy resin coating (Epoxy), waterborne epoxy resin coating doped with two-dimensional zinc phosphate sheet (Epoxy@ZPNS) and waterborne epoxy resin coating doped with multi-interface structured zinc phosphate particles (Epoxy@ZPNF).

Sample	Al alloy	Epoxy	Epoxy@ZPNS	Epoxy@ZPNF
R_s (ohm·cm^2)	20	20	20	20
CPE_{pa} (ohm $^{-1}$·cm^{-2}·s^n)	3.223×10^{-4}	–	–	–
n_{pa}	1	–	–	–
R_c (ohm·cm^2)	4.402×10^3	–	–	–
CPE_c (ohm $^{-1}$·cm^{-2}·s^n)	–	7.531×10^{-10}	8.067×10^{-11}	7.564×10^{-13}
	–			
n_c	–	0.8589	0.4169	1
R_c (ohm·cm^2)	–	8.090×10^4	1.154×10^5	2.161×10^7
CPE_{dl} (ohm $^{-1}$·cm^{-2}·s^n)	6.385×10^{-6}	4.788×10^{-6}	1.023×10^{-9}	2.146×10^{-13}
n_{dl}	0.9208	0.6731	0.7534	0.7216
R_{ct} (ohm·cm^2)	3.241×10^3	1.306×10^5	4.262×10^5	1.433×10^7
χ	1.3×10^{-4}	1.2×10^{-4}	2.7×10^{-4}	3.2×10^{-3}
Low-frequency impedance (ohm·cm^2)	5.28×10^3	9.73×10^4	3.29×10^5	3.74×10^7

lowest corrosion current density and the highest low-frequency impedance value, as presented in Fig. 2(f) [34–40].

3.3. *Long-term immersion corrosion behavior*

To test the long-term corrosion resistance, the waterborne epoxy resin coatings with and without zinc phosphate addition have been immersed in the 5 wt% NaCl solution for 3000 h. After immersion, the electrochemical performance of different coatings specimens were tested and the results are shown in Fig. 6 and Table 3. As shown in Fig. 6(a), the corrosion potential (E_{corr}) of the waterborne epoxy resin coating after immersion corrosion is −1.33 V, which have been decreased about 30% compared with the original coating. The corrosion current density (i_{corr}) of the waterborne epoxy resin coating after immersion corrosion is 4.17×10^{-4} A·cm^{-2}, which is increased about 2 orders of magnitude compared with the original coating. The corrosion potentials of the waterborne epoxy resin coatings doped with two-dimensional zinc phosphate sheets and multi-interface structured zinc phosphate particles changes little after immersion corrosion with values of −0.97 V and −0.74 V, respectively. However, the corrosion current density of the waterborne epoxy resin coating doped with two-dimensional zinc phosphate sheets increases to

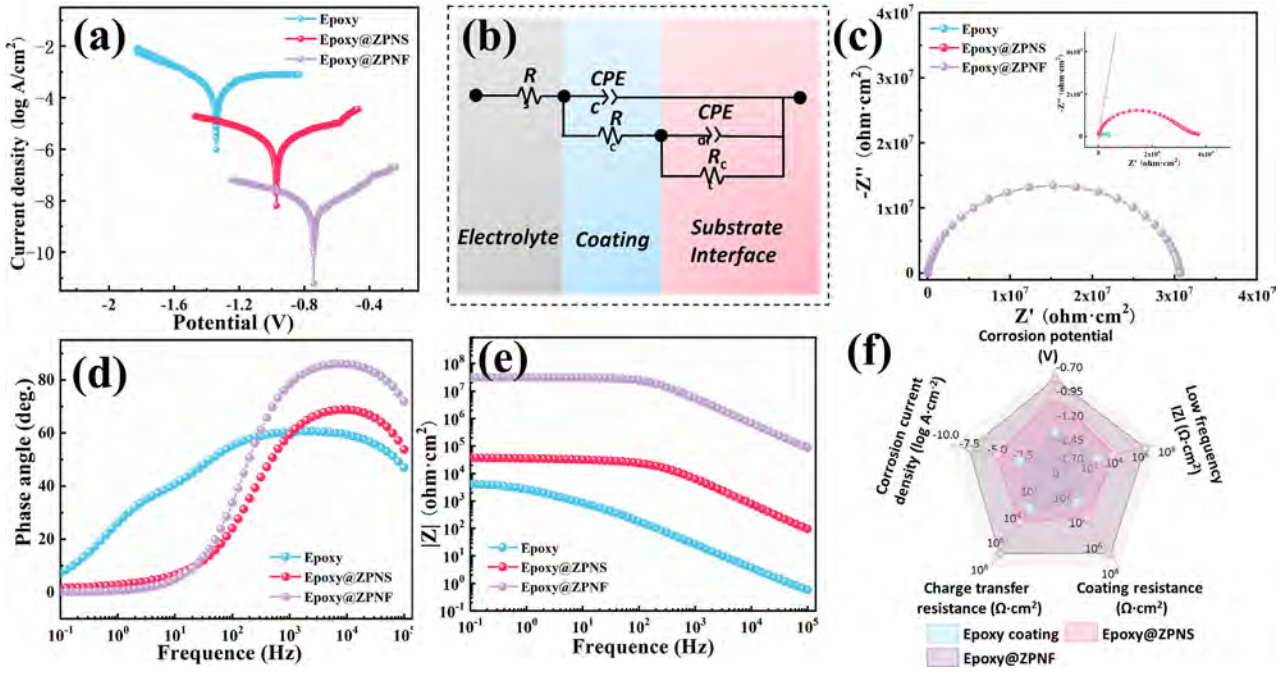

Fig. 6 – Electrochemical properties of waterborne epoxy resin coating (Epoxy), waterborne epoxy resin coating doped with two-dimensional zinc phosphate sheet (Epoxy@ZPNS) and waterborne epoxy resin coating doped with multi-interface structured zinc phosphate particles (Epoxy@ZPNF) specimens after immersion for 3000 h: (a) Tafel curve, (b) Fitting circuit, (c) Nyquist data, (d) Bode-absolute data, and (e) Bode-phase data, (f) Electrochemical performance.

Table 3 – Corrosion potentials and corrosion current densities of waterborne epoxy resin coating (Epoxy), waterborne epoxy resin coating doped with two-dimensional zinc phosphate sheet (Epoxy@ZPNS) and waterborne epoxy resin coating doped with multi-interface structured zinc phosphate particles (Epoxy@ZPNF) specimens after immersion.

Sample	E_{corr} (V)	i_{corr} (A·cm^{-2})
Epoxy	−1.33	4.17×10^{-4}
Epoxy@ZPNS	−0.97	3.24×10^{-6}
Epoxy@ZPNF	−0.74	5.75×10^{-9}

3.24×10^{-6} A·cm^{-2}, which increases 50% than that before immersion corrosion. It is interesting that the corrosion current density of the waterborne epoxy resin coating doped with multi-interface structured zinc phosphate particles almost has no changing. The evolution of corrosion potential and current density of the waterborne epoxy resin coatings indicates that the zinc phosphate addition could improve the protecting effect of the coating, especially the zinc phosphate with multi-interface structure, which could be attributed to its larger specific surface area. The coatings specimens were fitted using the equivalent circuit (EC) model R (Q (R (QR))), and the fitting circuit is shown in Fig. 6(b). The obtained electronic component values are summarized in Table 4. Fig. 6(c)–(e) shows the EIS test results, which have the same enhancement effect as Tafel curve. The specimen coated with multi-interface structured zinc phosphate particles doped coating demonstrates almost no change in the five main electrochemical performance indicators compared with its original state. While the specimen coated with two-dimensional zinc phosphate sheets doped coating showed a significant decrease in all performance indicators. As shown in Fig. 6(f), the electrochemical performance of the specimen coated with waterborne epoxy resin coating is close to that of the Al alloy substrate, which indicates its protecting effect is lost.

After 3000 h of immersion corrosion, it is found that zinc phosphate and its structure have influence the infiltration of corrosion medium obviously, as displayed in Fig. S7. The specimen coated with waterborne epoxy resin coating has been infiltrated thoroughly, while the specimen coated with two-dimensional zinc phosphate sheets doped waterborne epoxy resin coating has been infiltrated partly. The specimen coated with multi-interface structured zinc phosphate particles doped waterborne epoxy resin coating almost keeps the original state. Fig. 7 shows the distribution of elements on the surface of aluminum alloy after coating peeling. Clearly, there are many regions have experienced serious corrosion with fractured corroded products in the specimen coated with waterborne epoxy resin coating, as shown in Fig. 7(a) and (d). The brief elemental analyses reveal the corroded products are rich of Al and O. According to the SEM image in Fig. 7(b), it is found that there are some cracked corrosion pits on the surface of aluminum alloy coated with two-dimensional zinc phosphate sheets doped waterborne epoxy resin coating. The elemental analyses on the surface also indicate the obvious existence of O, as presented in Fig. 7(e). Different from the specimens coated with waterborne epoxy resin coating and two-dimensional zinc phosphate sheets doped coating, the Al alloy surface coated with multi-interface structured zinc phosphate particles doped waterborne epoxy resin coating still has the grinding trace, as shown in Fig. 7(c). The trace O content on the surface shown in Fig. 7(f) indicates that they mainly come from initial oxidation. Such a phenomenon implies the Al alloy coated with multi-interface structured zinc phosphate particles doped waterborne epoxy resin coating almost has no reaction with corrosion medium.

Table 4 – EIS fitting data of waterborne epoxy resin coating (Epoxy), waterborne epoxy resin coating doped with two-dimensional zinc phosphate sheet (Epoxy@ZPNS) and waterborne epoxy resin coating doped with multi-interface structured zinc phosphate particles (Epoxy@ZPNF) specimens after immersion.

Sample	Epoxy	Epoxy@ZPNS	Epoxy@ZPNF
CPE_c (ohm^{-1}·cm^{-2}·s^n)	2.113×10^{-5}	2.509×10^{-8}	1.822×10^{-12}
n_c	0.875	0.8413	0.9874
R_c (ohm·cm^2)	1.117×10^3	1.239×10^4	2.061×10^7
CPE_{dl} (ohm^{-1}·cm^{-2}·s^n)	6.811×10^{-4}	3.292×10^{-8}	1.718×10^{-12}
n_{dl}	0.723	0.9566	0.9202
R_{ct} (ohm·cm^2)	3.357×10^3	2.83×10^4	3.024×10^7
χ	4.9×10^{-4}	5.7×10^{-4}	1.2×10^{-3}
Low-frequency impedance (ohm·cm^2)	5.73×10^3	3.72×10^4	1.02×10^7

Fig. 8 is the XRD pattern of Al alloy specimens coated with different coatings after immersion corrosion for 3000 h. It can be found that the Al alloy specimens coated by waterborne epoxy resin coating and two-dimensional zinc phosphate sheet doped waterborne epoxy resin coating have formed Al_2O_3 oxides, as shown in Fig. 8(a) and (b). However, there are some difference. The strength of Al_2O_3 diffraction peaks in the Al alloy specimen coated by waterborne epoxy resin coating is stronger than those in the Al alloy specimen coated by two-dimensional zinc phosphate sheet doped waterborne epoxy resin coating, which indicates more Al_2O_3 oxides. It should be noted that there is almost no Al_2O_3 diffraction peaks in the Al alloy specimen coated by multi-interface structured zinc phosphate particles doped waterborne epoxy resin coating, as depicted in Fig. 8(c). That confirms the elemental analyses that there is no corrosion reaction in the Al alloy coated with multi-interface structured zinc phosphate particles doped waterborne epoxy resin coating. Combing with the electrochemical performance of the specimens coated with different coatings, it can be concluded that the zinc phosphate could play an important role during the inhibition of corrosion medium infiltration. The zinc phosphate not only provide the physical shielding to restrain the corrosion medium infiltration but also could provide the Zn ions to react with the corrosive medium, forming insoluble complex compounds [41]. In addition, the zinc phosphates with sheet or multi-interface structure both prefer to grow along (111) crystallographic place, which could provide the more stable interface and remains long-term shielding effect. Specifically, the multi-interface structured zinc phosphate particles have higher specific surface area than the zinc phosphate sheet, so the protecting effect of the multi-interface structured zinc phosphate particles doped waterborne epoxy resin coating is the best.

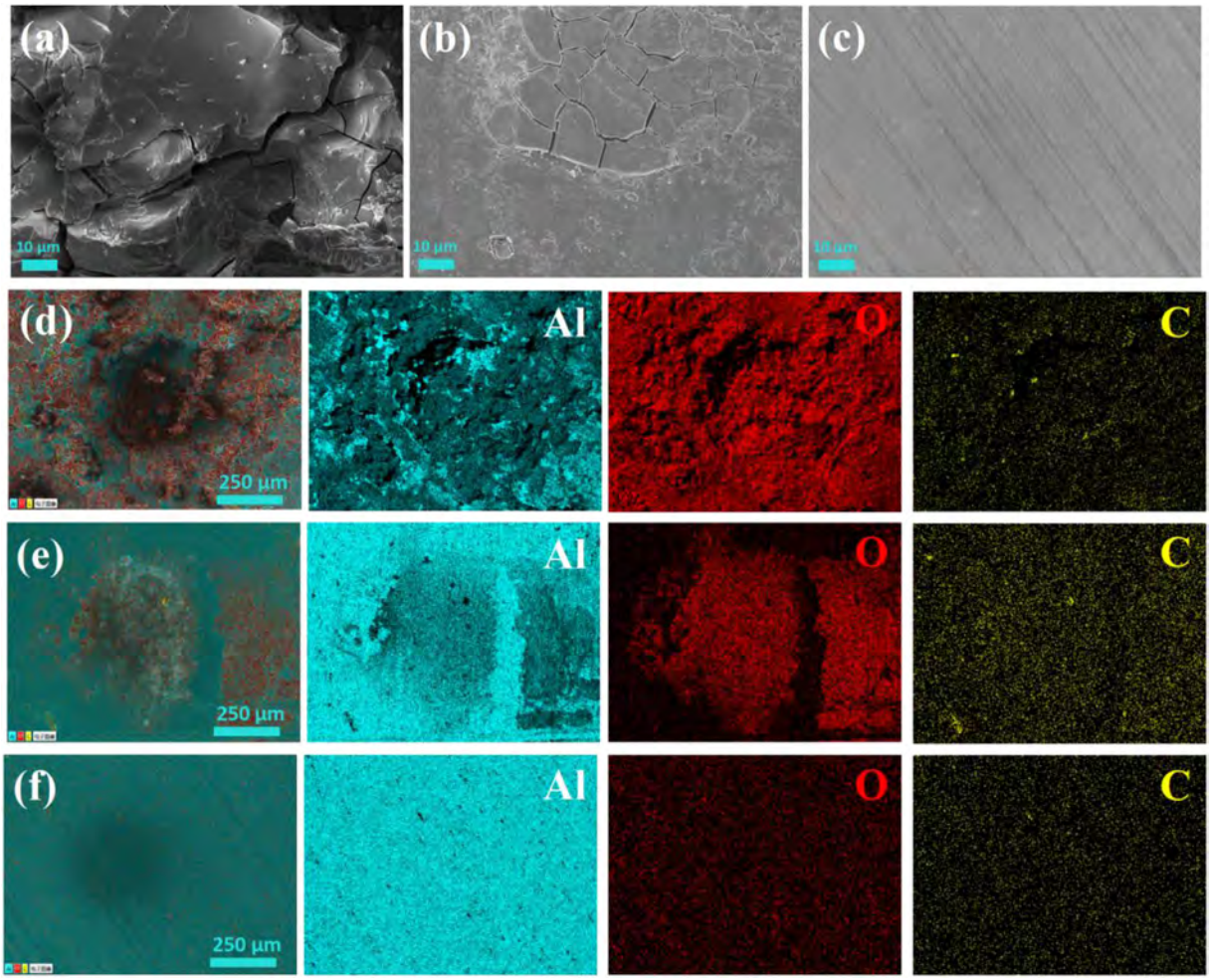

Fig. 7 – Typical surface morphology of the Al alloy surface peeling the coatings and elemental analysis after 3000 h immersion corrosion: (a) and (d) Specimen coated with waterborne epoxy resin coating (Epoxy), (b) and (e) Specimen coated with waterborne epoxy resin coating doped with two-dimensional zinc phosphate sheet (Epoxy@ZPNS), (c) and (f) Specimen coated with waterborne epoxy resin coating doped with multi-interface structured zinc phosphate particles (Epoxy@ZPNF).

3.4. *Adhesion strength*

Fig. 9 shows the adhesion strength of Al alloy specimens coated with different coating, and the test method is shown in Fig. S8. It can be seem that the adhesion strength of the initial waterborne epoxy resin coating is about 6.21 MPa, as shown in Fig. 9(a). The adhesion strength of the initial waterborne epoxy resin coatings doped with two-dimensional zinc phosphate sheets and multi-interface structured zinc phosphate particles is almost the same with the value about 6.81 MPa. After the 3000 h immersion corrosion, the adhesion strength of the waterborne epoxy resin coating is about 0.41 MPa, which decreases about 92% compared with its initial state. The adhesion strength of the waterborne epoxy resin coating doped with two-dimensional zinc phosphate sheets after immersion corrosion is about 2.3 MPa, which decreases about 65% than its initial state. It is interesting that the adhesion strength of the waterborne epoxy resin coating doped with multi-interface structured zinc phosphate particles after immersion corrosion is about 6.25 MPa, which just decreases about 8% than its initial state. Moreover, the adhesion strength of the waterborne epoxy resin coating doped with multi-interface structured zinc phosphate particles after immersion corrosion is still much higher than the application standard of the coating industry of 3.03 MPa (HG/T3668-2009). The comprehensive evaluation on three kinds of coating before and after long-term corrosion demonstrates that the waterborne epoxy resin coating doped with multi-interface structured zinc phosphate particles has the smallest performance degradation, while the waterborne epoxy resin coating has the highest performance degradation, as presented in Fig. 9(b). Such a performance variation should be attributed to the inhibition effect of zinc phosphate. The better inhibition effect, the fewer interfacial corrosion product and the higher adhesion strength.

3.5. *Influence of zinc phosphate structure on corrosion mechnism*

According to the previous researches [42–44], the small-size additive in the waterborne coating mainly plays the inhibition role during the corrosion. By the physical inhibition, the

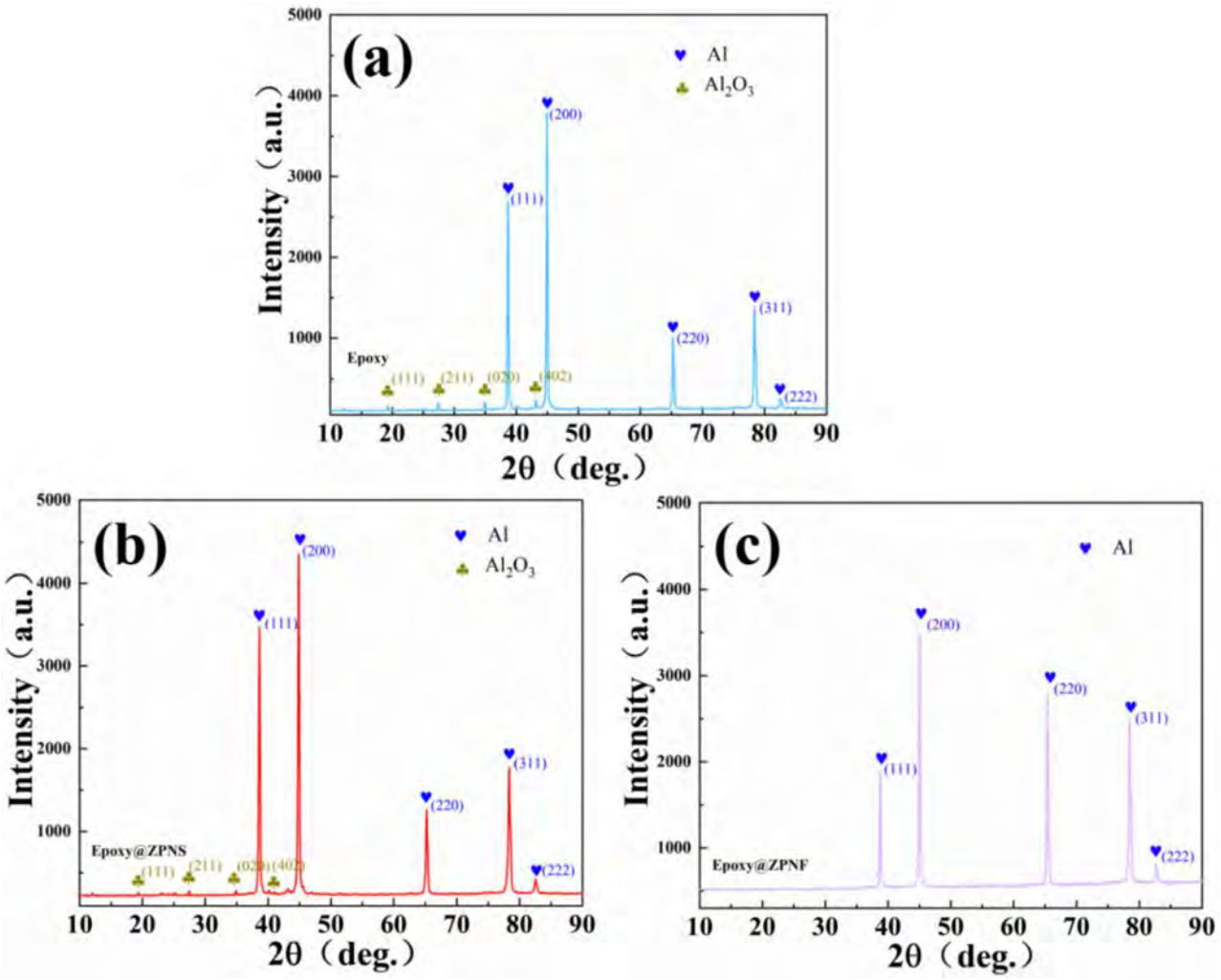

Fig. 8 – The XRD patterns of the Al alloy surface peeling the coatings after 3000 h immersion corrosion: (a) Specimen coated with waterborne epoxy resin coating (Epoxy), (b) Specimen coated with waterborne epoxy resin coating doped with two-dimensional zinc phosphate sheet (Epoxy@ZPNS), (c) Specimen coated with waterborne epoxy resin coating doped with multi-interface structured zinc phosphate particles (Epoxy@ZPNF).

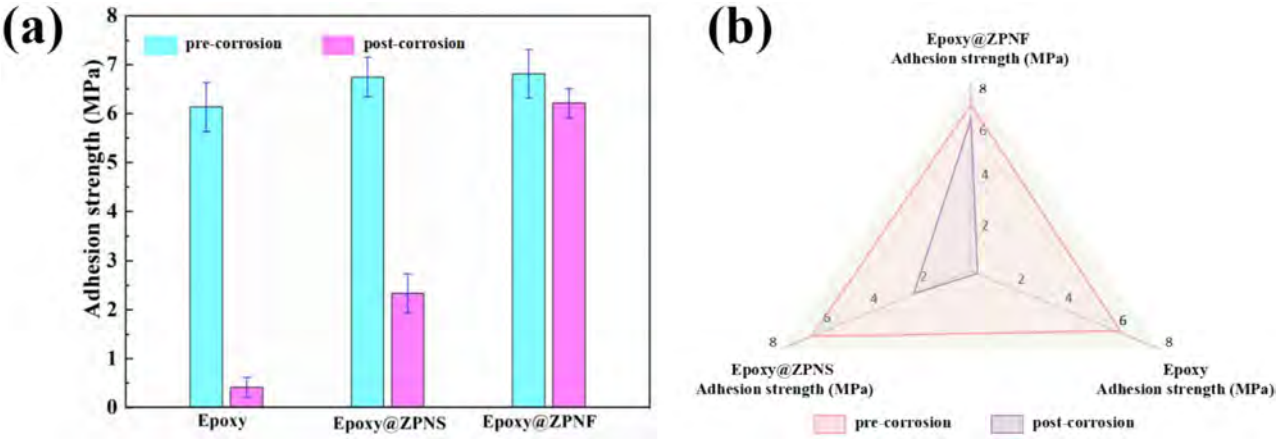

Fig. 9 – (a) Adhesion strength of the coatings before and after 3000 h immersion corrosion, (b) Comprehensive evaluation on the coatings.

corrosion medium infiltration could be restrained, which could extent the effective protection time of the coating and postpone the matrix corrosion. In the present research, the waterborne epoxy resin coating could isolate the Al alloy substrate from the corrosion medium, but the existence of polar channels result in the infiltration of corrosion medium, as shown in Fig. 10(a). Since the formation of polar channels originated from curing stress, they demonstrate the random distribution, which could impede the infiltration. However, the infiltrated corrosion medium would accelerate the aging of epoxy resin molecular and finally connect the adjacent polar channel. Though the infiltration process costs time, once the corrosion medium comes to the Al alloy substrate, the inner corrosion would begin. The formed Al_2O_3 corrosion products would increase the interfacial stress, which destroys the adhesion of coating until it is peeled. After then, the inner

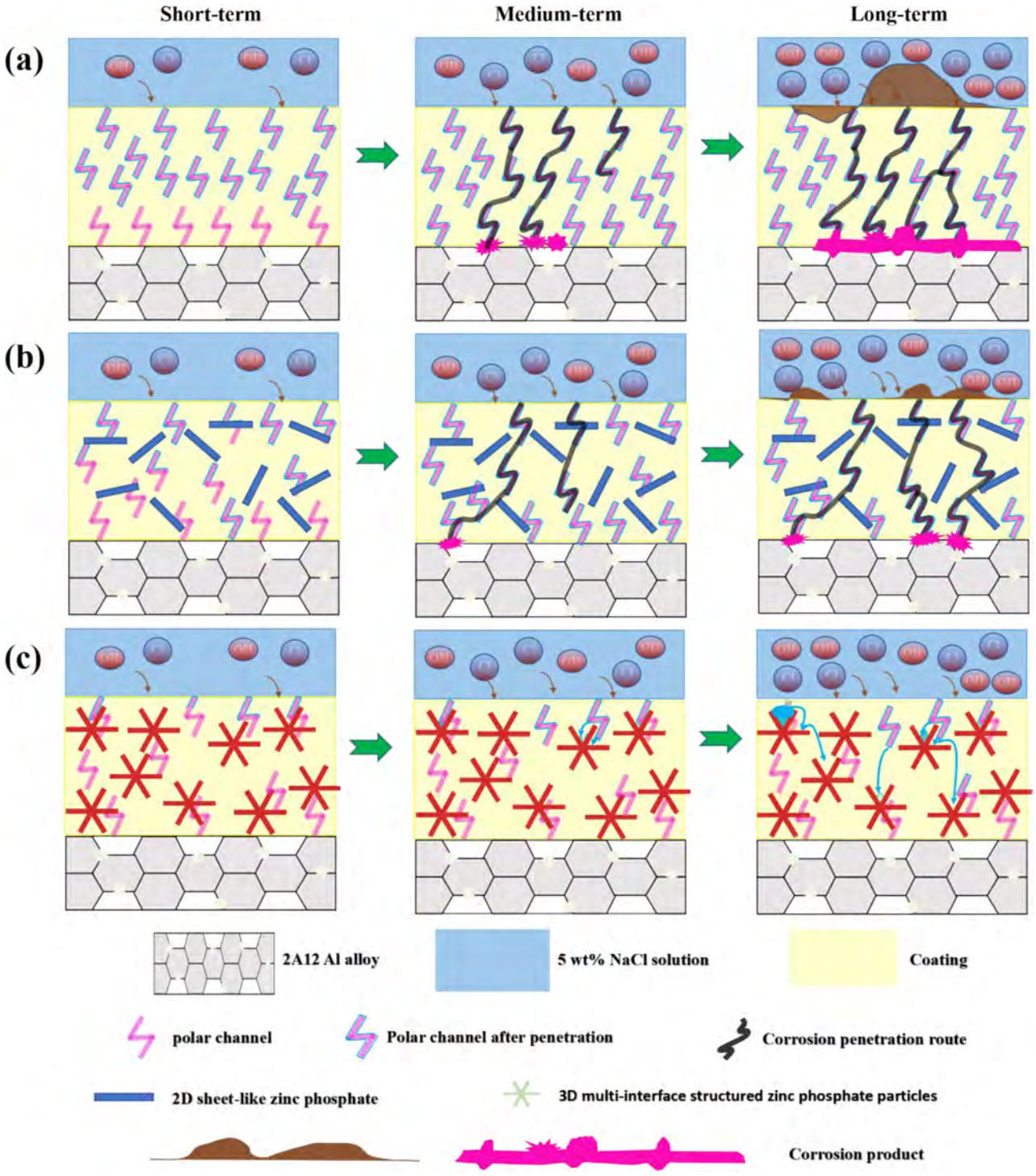

Fig. 10 – Schematic diagram of corrosion mechanism of the coatings: (a) waterborne epoxy resin coating (Epoxy), (b) waterborne epoxy resin coating doped with two-dimensional zinc phosphate sheet (Epoxy@ZPNS), (c) waterborne epoxy resin coating doped with multi-interface structured zinc phosphate particles (Epoxy@ZPNF).

corrosion would be amplified gradually till the coating is locally destroyed.

Fig. 10(b) shows that the addition of zinc phosphate changes the infiltration process of corrosive media through inhibition. For the tow-dimensional zinc phosphate sheets, their lamellar shape helps to cut off the polar channel in the waterborne epoxy resin coating and prolong the infiltration path [45,46]. Moreover, the added zinc phosphate sheets also relieve the curing stress by the breaking of long molecular cross-linking, which helps to decrease the polar channel. Even though the zinc phosphate sheet could react with the corrosion medium forming insoluble complex compounds, however, the corrosion medium still could bypass the zinc phosphate sheets after a certain time, because of its simple interface shape. Therefore, the tow-dimensional zinc phosphate sheets doped waterborne epoxy resin coating have better immersion corrosion resistance than that of the waterborne epoxy resin coating, but it still suffers some damage during the 3000 h long-term immersion corrosion. In contrast, the multi-interface structured zinc phosphate particles have three-dimensional interface and large specific surface area, which could take full use of the spatial structure to impede the infiltration of corrosion medium, as shown in Fig. 10(c). Furthermore, the multi-interface structured zinc phosphate particles could relieve the curing stress better, because its three-dimensional structure exerts little orientation preference. Combing with its good filling effect, the multi-interface structured zinc phosphate particles would decrease the polar channels in waterborne epoxy resin coating more effectively. Therefore, the corrosion medium is well locked by the multi-interface structured zinc phosphate particles and difficult to reach the Al alloy substrate. Then, it can be concluded that it is the cooperation of strengthened physical inhibition effect, decreased polar channel and complexation reaction in multi-interface structured zinc phosphate particles doped waterborne epoxy resin coating that ensue the well improved corrosion resistance [41]. Such a multi-functional synergistic thoughts provides a method to design the environment-friendly corrosion resistance coating for offshore application.

4. Conclusions

In the present research, the multi-interface structured zinc phosphate particle with large specific surface area was prepared by regulating the zinc phosphate crystal growth process, which was applied to develop a epoxy-based waterborne coating with better corrosion resistance. Its electrochemical properties and immersion corrosion behavior were investigated comparing with waterborne epoxy resin coating and two-dimensional zinc phosphate sheets doped waterborne epoxy resin coating. Some conclusion can be drawn as below.

(1) The synthesized multi-interface structured zinc phosphate particles have diameter about 2–5 μm and comprise many nanosheets with thickness of 10–50 nm. Moreovoer, the multi-interface structured zinc phosphate particles prefer to grow along (111) crystallographic plane and have more crystallization water, which may be beneficial to their interficial bonding with epoxy resin and corrosion resistance.
(2) The addition of two-dimension zinc phosphate sheets and multi-interface structured zinc phosphate particles could decrease the micropore and promote the flatting of the waterborne epoxy resin coating. Compared with the waterborne epoxy resin coatings doped with and without two-dimensional zinc phosphate sheet, the multi-interface structured zinc phosphate particles doped waterborne coating has highest corrosion potential (−0.73 V), lowest corrosion current density (3.98×10^{-9} A/cm^2) and the highest low-frequency impedance (3.74×10^7 ohm cm^2), which indicates the obvious benefit of multi-interface structured zinc phosphate particles on corrosion resistance of waterborne epoxy resin coating.
(3) After 3000 h immersion corrosion in 5 wt% NaCl solution, the electrochemical properties waterborne epoxy resin coatings doped with and without two-dimensional zinc phosphate sheets have decreased significantly, but those of multi-interface zinc phosphate particles doped waterborne epoxy resin coating just decrease a little with corrosion potential of −0.74 V, corrosion current density of 5.75×10^{-9} A/cm^2, low-frequency impedance of over 3.024×10^7 ohm cm^2. In addition, the multi-interface zinc phosphate particles doped waterborne epoxy resin coating after long-term immersion corrosion still has the adhesion strength of 6.21 MPa, while the other coatings has lost 66–92% adhesion strength. The well improved corrosion resistance of multi-interface structured zinc phosphate particles doped waterborne epoxy resin coating should be attributed to the cooperation of strengthened physical inhibition effect, decreased polar channel and complexation reaction.

Declaration of Competing Interest

The authors declare that they have no known competing financial interests or personal relationships that could have appeared to influence the work reported in this paper.

Acknowledgements

This work was supported by 2022 Shenzhen sustainable supporting funds for colleges and universities (20220810143642004), Shenzhen Science and Technology Research (SGDX20201103095406024), Shenzhen Basic Research Project (JCYJ20200109144608205 and JCYJ20210324120001003), Guangdong Basic and Applied Basic Research Foundation (2020A1515011301, 2019A1515110067, and 2020A1515110055), Peking University Shenzhen Graduate School Research Start-up Fund of Introducing Talent (1270110273), Shenzhen post-doctoral research fund project after outbound (2129933651), City University of Hong Kong Strategic Research (SRG No. 7005505), Shenzhen - Hong Kong Technology Cooperation Funding Scheme (TCFS) GHP/149/20SZ (CityU 9440296), City

University of Hong Kong Donation Research (DON-RMG No. 9229021), and Project funded by China Postdoctoral Science Foundation (2023M730032).

Appendix A. Supplementary data

Supplementary data to this article can be found online at https://doi.org/10.1016/j.jmrt.2023.09.109.

REFERENCES

[1] Tong HT, Liu XH, Liu YP, Zhang HX, Li XB. Electrochemical investigation of the corrosion inhibiting effect of organic paints doped with benzotriazole coated on steel substrates. Corrosion Eng Sci Technol 2021;56:618–25.

[2] Zheng DJ, Gui Q, Xu YQ, Song GL. Modified AC-DC-AC method for evaluation of corrosion damage of acrylic varnish paint coating/Q215 steel system. Prog Org Coating 2021;159:106401.

[3] Yang C, Cui SH, Weng YC, Wu ZC, Liu LL, Ma ZY, et al. Scalable superhydrophobic T-shape micro/nano structured inorganic alumina coatings. Chem Eng J 2021;409:128142.

[4] Yu M, Dong H, Shi HB, Xiong LL, He C, Liu JH, et al. Effects of graphene oxide-filled sol-gel sealing on the corrosion resistance and paint adhesion of anodized aluminum. Appl Surf Sci 2019;479:105–13.

[5] Torknezhad Y, Khosravi M, Assefi M. Corrosion protection performance of nanoparticle incorporated epoxy paint assessed by linear polarization and electrochemical impedance spectroscopy. Mater Corros 2018;69:472–80.

[6] Olender J, Jarkiewicz KW. Extraction of zinc corrosion from beneath a paint layer: a case study. Stud Conserv 2019;64:146–58.

[7] Cui MJ, M Ren S, Zhao HC, Xue QJ, P Wang L. Polydopamine coated graphene oxide for anticorrosive reinforcement of water-borne epoxy coating. Chem Eng J 2018;335:255–66.

[8] Tjahjanti PH, Hidayat AR, Firdaus R, Iswanto, Nurcahyo R, Fitri GAN. Study on the making of corrosion resistant steel (ASTM A36 Steel) coatings from a mix of graphene oxide + waterborne paint. IOP Conf Ser Mater Sci Eng 2019;673:012122.

[9] Ehsanjoo M, Mohammadi S, Chaibakhsh N. Long-term corrosion resistance of zinc-rich paint using functionalised multi-layer graphene-tripolyphosphate: in situ creation of zinc phosphate as corrosion inhibitor. Corrosion Eng Sci Technol 2019;54:698–714.

[10] LeBozec N, Thierry D, Pelissier K. A new accelerated corrosion test for marine paint systems used for ship's topsides and superstructures. Mater Corros 2018;69:447–60.

[11] Wang SD, Lamborn L, Chen WX. Near-neutral pH corrosion and stress corrosion crack initiation of a mill-scaled pipeline steel under the combined effect of oxygen and paint primer. Corrosion Sci 2021;187:109511.

[12] Silva MDN, Kassab E, Pandoli OG, Oliveira JLD, Quintela JP, Bott IS. Corrosion behaviour of an epoxy paint reinforced with carbon nanoparticles. Corrosion Eng Sci Technol 2020;55:603–8.

[13] Wang SD, Lamborn L, Chevil K, Gamboa E, Chen WX. Near-neutral pH corrosion of mill-scaled X-65 pipeline steel with paint primer. J Mater Sci Technol 2020;49:166–78.

[14] Selvaraj V, R Raghavarshini T, Alagar M. Evaluation of thermo-mechanical, dielectric and corrosion resistant properties of cardanol benzoxazine-epoxy based hybrid composites: a very low temperature curing pre-polymer for high performance paint related applications. High Perform Polym 2020;32:524–39.

[15] Bahçe E, Demire MH, Köytepe S, Seçkin T. Production of abrasive apricot kernel shell powder/boron nitride/polyester composites for cleaning of paint and corrosion on metal surfaces. Polym Compos 2020;41:544–55.

[16] Contri G, Zimmermann CA, Ramoa SDADS, Schmitz DP, Fedel M. Polypyrrole modified e-coat paint for corrosion protection of aluminum AA1200. Front. Mater. 2020;7:45–53.

[17] Bahçe E, Demirel MH, Köytepe S, Seçkin T. Production of abrasive apricot kernel shell powder/boron nitride/polyester composites for cleaning of paint and corrosion on metal surfaces. Polym Compos 2020;41:544–55.

[18] Ren HS, Li T, Wang HG, Guo ZH, Chen TL, Meng FB. Two birds with one stone: superhelical chiral polypyrrole towards high-performance electromagnetic wave absorption and corrosion protection. Chem Eng J 2022;427:131582.

[19] Yu F, Wang K, Cui L, Wang S, Hou M, Xiong F, et al. Vertical-graphene-reinforced titanium alloy bipolar plates in fuel cells. Adv Mater 2022;34:2110565.

[20] Liu CB, Zhao HC, Hou PM, Qian B, Wang X, Guo CY, et al. Efficient graphene clodextrin based nanocontainer:synthesis and host-guest inclusion for self-healing anticorrosion application. ACS Appl Mater Interfaces 2018;10:36229.

[21] Naguib M, Kurtoglu M, Presser V, Lu J, Niu J, Min H, et al. Two-dimensional nanocrystals two-dimensional nanocrystals produced by exfoliation of Ti_3AlC_2. Adv Mater 2011;23:4248–53.

[22] Yan H, Wang J, Meng C, Wang X, Zhu MH. Towards long-term corrosion and wear protection of Al alloy: synergy of $Ti_3C_2T_x$ flake and micro-arc oxidation coating. Corrosion Sci 2020;174:108813.

[23] Yan H, Zhang L, Li H, Fan XQ, Zhu MH. Towards high-performance additive of Ti_3C_2 graphene hybrid with a novel wrapping structure in epoxy coating. Carbon 2019;157:217–33.

[24] Yan H, Cai M, Li W, Fan XQ, Zhu MH. Amino-functionalized Ti_3C_2 with anti-corrosive wear function for waterborne epoxy coating. J Mater Sci Technol 2020;54:144–59.

[25] Shen L, Zhao Y, Wang Y, Song R, Yao Q, Chen S, et al. Long-term corrosion barrier with insulating boron nitride monolayer, Corrigendum to Processable poly(2-butylaniline) hexagonal boron nitride nanohybrids for synergetic anticorrosive reinforcement of epoxy coating. J Mater Chem A 2016;4:5044–50.

[26] Cui MJ, Ren SM, Qin SL, Xue QJ, Zhao HC, Wang LP. Corrigendum to processable poly(2-butylaniline)hexagonal boron nitride nanohybrids for synergetic anticorrosive reinforcement of epoxy coating. Corrosion Sci 2022;194:109922.

[27] Yang C, Cai H, Cui SH, Huang J, Zhu JY, Wu ZC, et al. A zinc-doped coating prepared on the magnesium alloy by plasma electrolytic oxidation for corrosion protection. Surf Coating Technol 2022;433:128148.

[28] Yang C, Cui SH, Wu ZC, Zhu JY, Huang J, Ma ZY, et al. High efficient co-doping in plasma electrolytic oxidation to obtain long-term self-lubrication on Ti_6Al_4V. Tribol Int 2021;160:107018.

[29] Yang C, Zhu JY, Cui SH, Chen PH, Wu ZC, Ma ZY, et al. Wear and corrosion resistant coatings prepared on LY12 aluminum alloy by plasma electrolytic oxidation. Surf Coating Technol 2021;409:126885.

[30] Xu RX, Xu DW, Zeng Z, Liu D. $CoFe_2O_4$/porous carbon nanosheet composites for broadband microwave absorption. Chem Eng J 2022;427:130796.

[31] Lindell D, Pettersson R. Crystallographic effects in corrosion of austenitic stainless steel 316L. Mater Corros 2015;66(8):727–32.

[32] Ji HC, Zeng W, Li YQ. Facile synthesis of novel MoO_3 nanoflowers for high-performance gas sensor. J Mater Sci Mater Electron 2019;30:6601–7.
[33] Takahashi M, Deguchi H, Hayashi Y, Kimura A, Hanaki K, Tsuchiya H, et al. Corrosion behavior of carbon steel coated with a zinc-rich paint containing metallic compounds under wet and dry cyclic conditions. Mater Corros 2021;72. 1787-1786.
[34] Sobolev A, Bograchev D, Borodianskiy K, Zinigrad M. Kinetics and mechanism of corrosion of oxide coating fabricated on aluminum alloy by the plasma electrolytic oxidation in molten salt. Corrosion Sci 2022;208:110604.
[35] Schem M, Schmidt T, Gerwann J, Wittmar M, Veith M, Thompson GE, et al. CeO_2-filled sol-gel coatings for corrosion protection of AA2024-T3 aluminium alloy. Corrosion Sci 2009;51:2304–15.
[36] Wen L, Wang YM, Zhou Y, Ouyang JH, Guo LX, Jia DC. Corrosion evaluation of microarc oxidation coatings formed on 2024 aluminium alloy. Corrosion Sci 2010;52:2687–96.
[37] Nooshabadi MS, Ghoreishi SM, Behpour M. Direct electrosynthesis of polyaniline-montmorrilonite nanocomposite coatings on aluminum alloy 3004 and their corrosion protection performance. Corrosion Sci 2011;53:3035–42.
[38] Valdez B, Kiyota S, Stoytcheva M, Zlatev R, Bastidas JM. Cerium-based conversion coatings to improve the corrosion resistance of aluminium alloy 6061-T6. Corrosion Sci 2014;87:141–9.
[39] Wang J, Meng L, Zhang Z, Sa B, Fu X, Sheng L, et al. Investigation on the crystal structure and mechanical properties of the ternary compound Mg11-xZnxSr combined with experimental measurements and first-principles calculations. J Magnesium Alloys 2023;11:1074–82.
[40] Ravnikara D, Rajamureb RS, Trdana U, Dahotreb NB, Gruma J. Electrochemical and DFT studies of laser-alloyed TiB_2/TiC/Al coatings on aluminium alloy. Corrosion Sci 2018;136:18–27.
[41] C. Yang, J. Huang, S. H. Cui, R. K. Y. Fu, L. Y. Sheng, D. K. Xu, et al.. NaF assisted preparation and the improved corrosion resistance of high content ZnO doped plasma electrolytic oxidation coating on AZ31B alloy, J Magnesium Alloys. https://doi.org/10.1016/j.jma.2023.02.008.
[42] Wu YM, Yu JJ, Zhao WJ, Wang CT, Wu B, Lu GM. Investigating the anti-corrosion behaviors of the waterborne epoxy composite coatings with barrier and inhibition roles on mild steel. Prog Org Coating 2019;133:8–18.
[43] Dhoke SK, Khanna AS. Effect of nano-Fe_2O_3 particles on the corrosion behavior of alkyd based waterborne coatings. Corrosion Sci 2009;51:6–20.
[44] Wan HX, Song DD, Li XG, Zhang DW, Gao J, Du CW. Effect of zinc phosphate on the corrosion behavior of waterborne acrylic coating/metal interface. Materials 2017;10:654.
[45] Sheng CH, Cheng LH, Chen X, Zhang YH, Guo WH. Synergistic effect of 2D/0D mixed graphitic carbon nitride/Fe_2O_3 on the excellent corrosion behavior of epoxy-based waterborne coatings. Colloid Polym Sci 2021;299:883–97.
[46] J. Wang, L. Meng, W. Xie, C. Ji, R. Wang, P. Zhang, et al.. Corrosion and in vitro cytocompatibility investigation on the designed Mg-Zn-Ag metallic glasses for biomedical application, J Magnesium Alloys. https://doi.org/10.1016/j.jma.2022.09.025.

A high corrosion-resistant waterborne epoxy resin coating improved by addition of multi-interface structured zinc phosphate particles

Hu Cai[a,1], Xiteng Li[a,1], Yulin Zhang[a], Chao Yang[a], Suihan Cui[a,*], Liyuan Sheng[b,c,*], Daokui Xu[d], Ricky K. Y. Fu[e], Xiubo Tian[a], Paul K. Chu[e], Zhongzhen Wu[a,*]

[a] School of Advanced Materials, Peking University Shenzhen Graduate School, Shenzhen 518055, China

[b] Shenzhen Institute, Peking University, Shenzhen 518057, China

[c] PKU-HKUST ShenZhen-HongKong Institution, Shenzhen 518057, China

[d] Key Laboratory of Nuclear Materials and Safety Assessment, Institute of Metal Research, Chinese Academy of Sciences, Shenyang 110016, China

[e] Department of Physics, Department of Materials Science & Engineering, and Department of Biomedical Engineering, City University of Hong Kong, Tat Chee Avenue, Kowloon, Hong Kong, China

[*] Corresponding author. E-mail address: cuish@pku.edu.cn (S. Cui); lysheng@yeah.net (L. Sheng); wuzz@pku.edu.cn (Z. Wu)

[1] These authors contributed equally to this work.

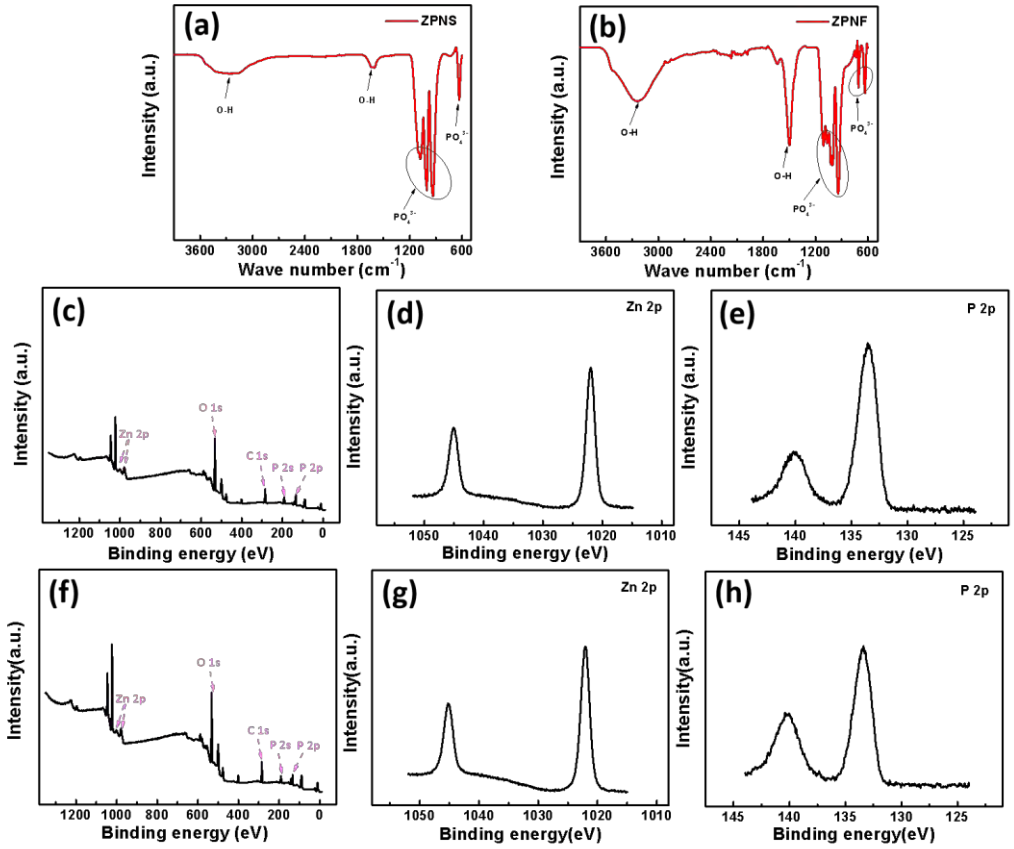

Fig. S1. Characterization of the two-dimensional zinc phosphate sheet: (a) FTTR spectrum; XPS spectra: (c) Survey, (d) Zn 2*p*, and (e) P 2*p*; Characterization of multi-interface structured zinc phosphate particles: (b) FTTR spectrum; XPS spectra: (f) Survey, (g) Zn 2*p*, and (h) P 2*p*.

2*p*.

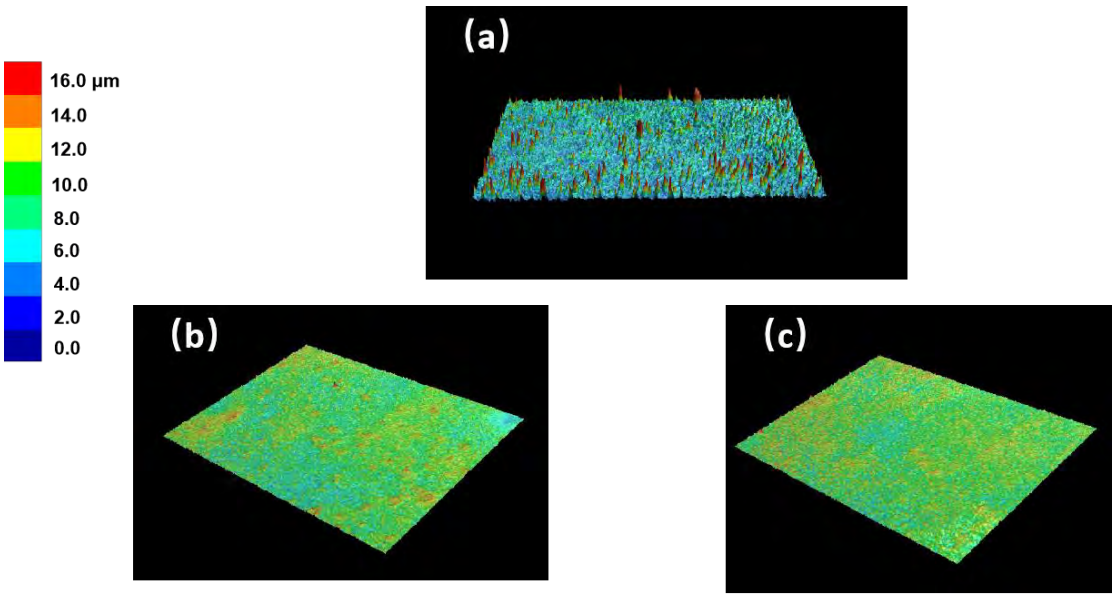

Fig. S2. The three-dimensional morphology observations on the waterborne epoxy resin coatings by LCSM: (a) waterborne epoxy resin coating, (b) waterborne epoxy resin coating doped with two-dimensional zinc phosphate sheet, (c) waterborne epoxy resin coating doped with multi-interface structured zinc phosphate particles.

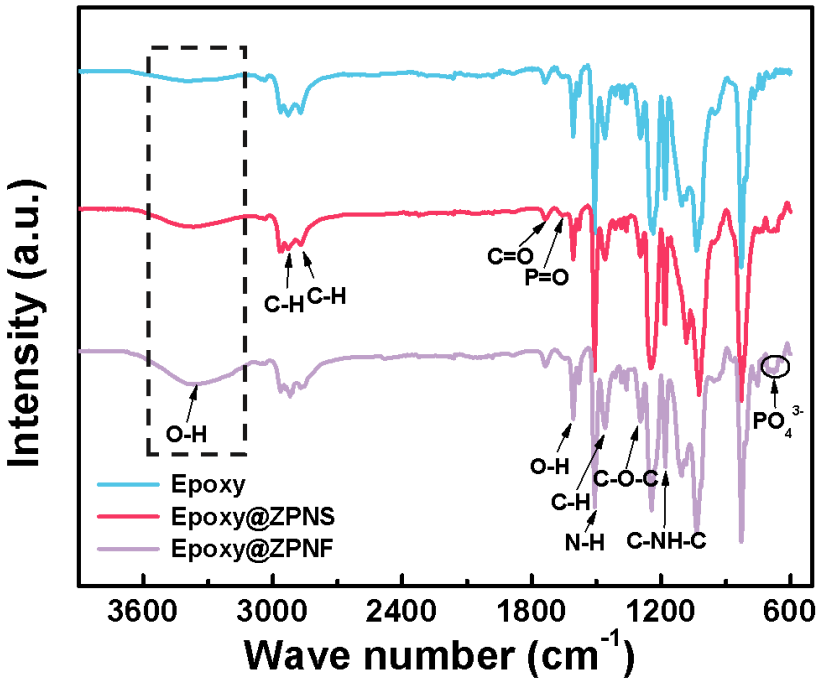

Fig. S3. FTIR spectra of the waterborne epoxy resin coating (Epoxy), waterborne epoxy resin coating doped with two-dimensional zinc phosphate sheet (Epoxy@ZPNS) and waterborne epoxy resin coating doped with multi-interface structured zinc phosphate particles (Epoxy@ZPNF).

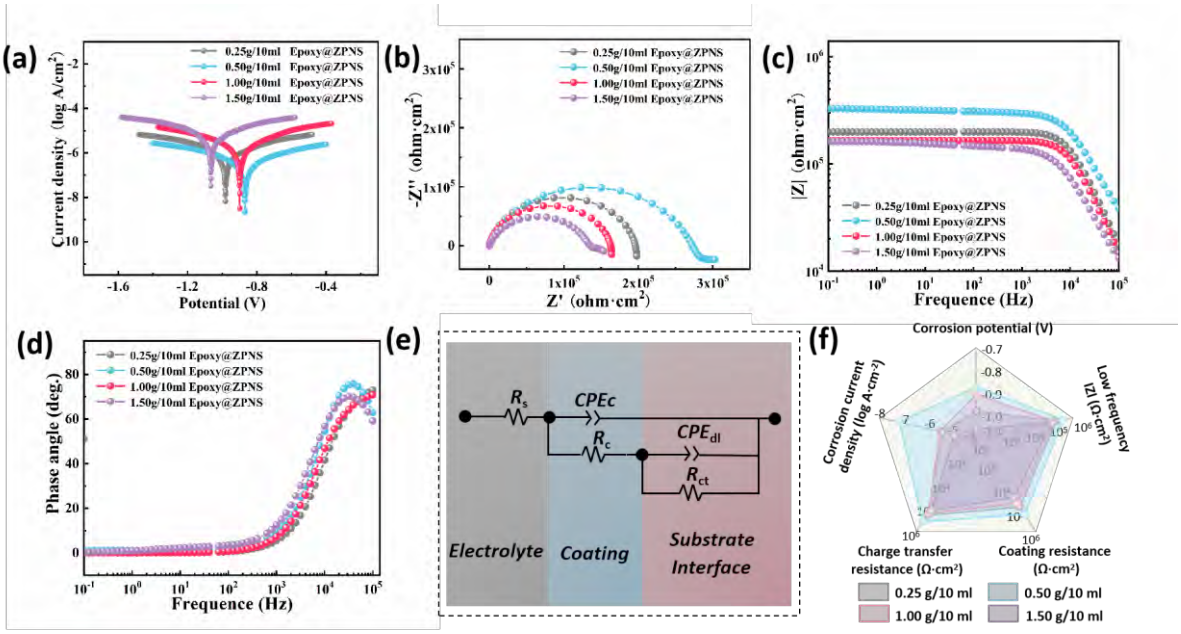

Fig. S4. Electrochemical properties of waterborne epoxy resin coating doped with two-dimensional zinc phosphate sheet (Epoxy@ZPNS) with different concentrations: (a) Tafel curve, (b) Nyquist data, (c) Bode-absolute data, (d) Bode-phase data, (e) Fitting circuit, and (f) Electrochemical performance.

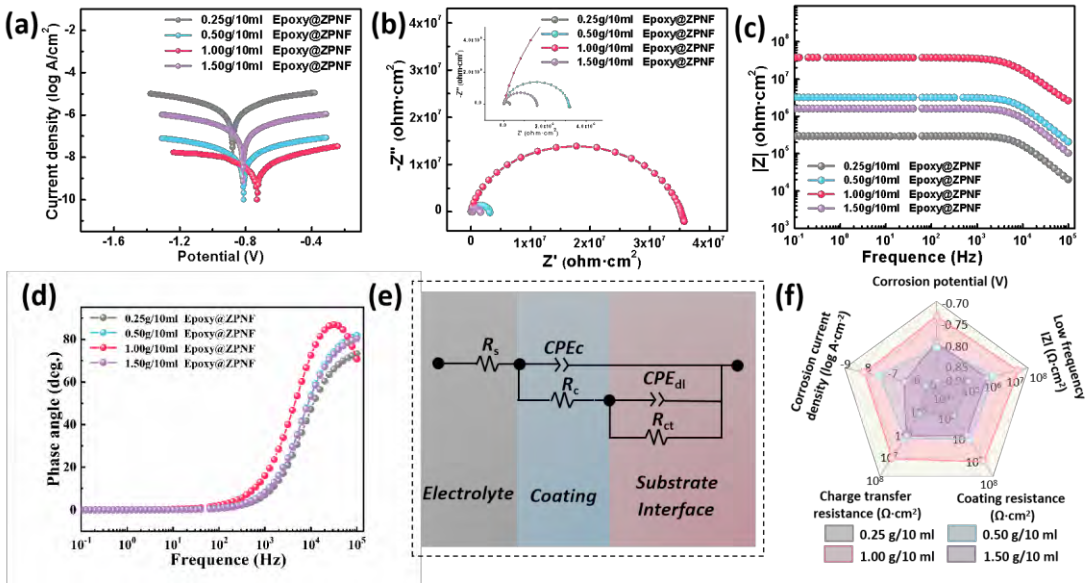

Fig. S5. Electrochemical properties of waterborne epoxy resin coating doped with multi-interface structured zinc phosphate particles (Epoxy@ZPNF) with different concentrations: (a) Tafel curve, (b) Nyquist data, (c) Bode-absolute data, (d) Bode-phase data, (e) Fitting circuit, and (f) electrochemical performance.

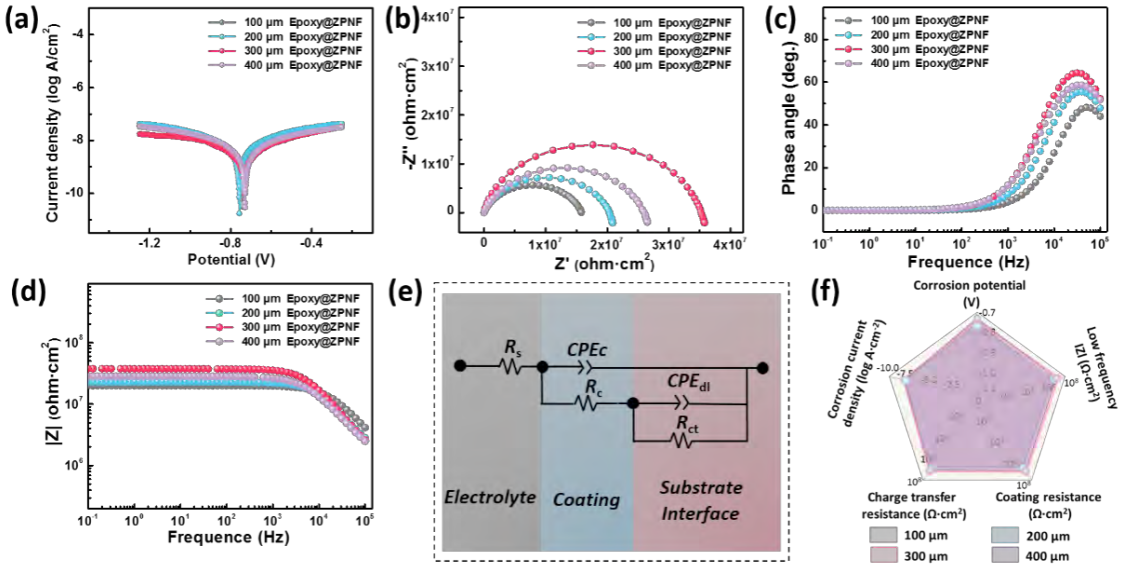

Fig. S6. Electrochemical properties of waterborne epoxy resin coating doped with multi-interface structured zinc phosphate particles (Epoxy@ZPNF) with different thicknesses: (a) Tafel curve, (b) Nyquist data, (c) Bode-phase data, (d) Bode-absolute data, (e) Fitting circuit, and (f) Electrochemical performance.

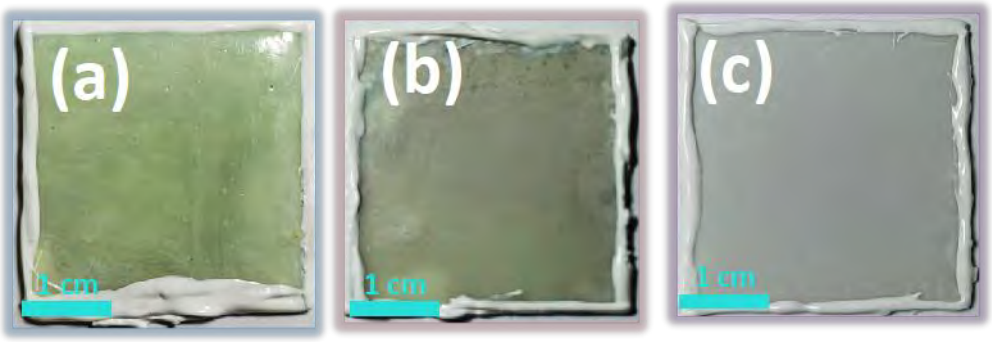

Fig. S7. Optical macrograph of the (a) waterborne epoxy resin coating (Epoxy), (b) waterborne epoxy resin coating doped with two-dimensional zinc phosphate sheet (Epoxy@ZPNS) and (c) waterborne epoxy resin coating doped with multi-interface structured zinc phosphate particles (Epoxy@ZPNF) after salt solution immersion corrosion for 3000 hours.

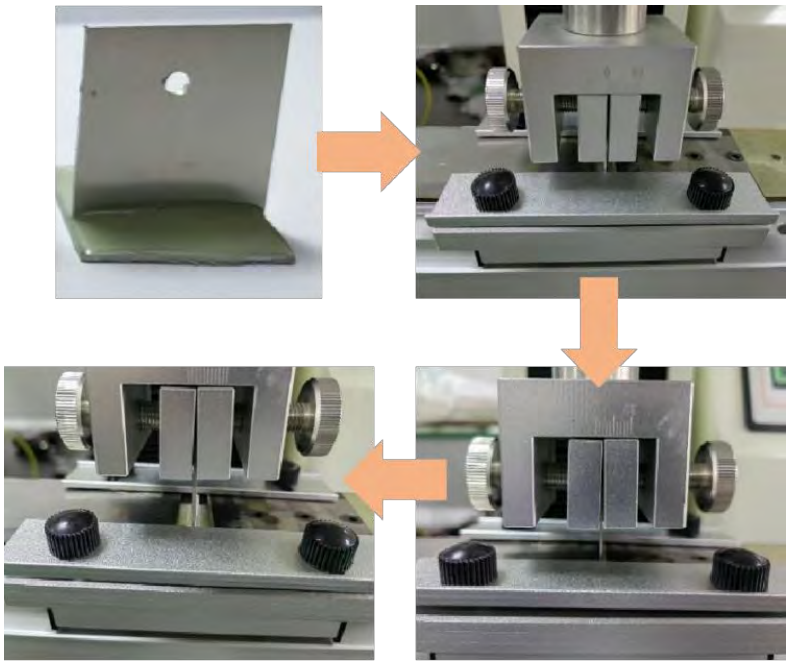

Fig. S8. The process of adhesion strength between Al alloy substrates and the waterborne epoxy resin coatings.

Table S1 Corrosion potentials and corrosion current densities of waterborne epoxy resin coating doped with two-dimensional zinc phosphate sheet (Epoxy@ZPNS) with different concentrations.

Sample	E_{corr} (V)	i_{corr} (A·cm^{-2})
0.25 g	-0.97	1.74×10^{-6}
0.50 g	-0.87	6.11×10^{-7}
1.00 g	-0.90	1.58×10^{-6}
1.50 g	-1.06	1.00×10^{-5}

Table S2 EIS fitting data of waterborne epoxy resin coating doped with two-dimensional zinc phosphate sheet (Epoxy@ZPNS) with different concentrations.

Sample	0.25 g	0.50 g	1.00 g	1.50 g
CPE_c ($ohm^{-1}\cdot cm^{-2}\cdot s^n$)	9.967×10^{-11}	8.067×10^{-11}	1.070×10^{-10}	4.494×10^{-10}
n_c	0.9416	0.4169	0.8927	0.9182
R_c ($ohm\cdot cm^2$)	9.911×10^{4}	1.154×10^{5}	9.355×10^{4}	6.347×10^{4}
CPE_{dl} ($ohm^{-1}\cdot cm^{-2}\cdot s^n$)	2.517×10^{-9}	1.023×10^{-9}	3.053×10^{-7}	2.945×10^{-6}
n_{dl}	0.8001	0.7534	0.8114	0.5412
R_{ct} ($ohm\cdot cm^2$)	2.057×10^{5}	4.262×10^{5}	1.197×10^{5}	1.151×10^{5}
χ	3.3×10^{-3}	2.7×10^{-4}	1.7×10^{-3}	1.2×10^{-4}

Table S3 Corrosion potentials and corrosion current densities of waterborne epoxy resin coating doped with multi-interface structured zinc phosphate particles (Epoxy@ZPNF) with different concentrations.

Sample	E_{corr} (V)	i_{corr} ($A\cdot cm^{-2}$)
0.25 g	-0.88	1.86×10^{-6}
0.50 g	-0.80	1.58×10^{-8}
1.00 g	-0.73	3.98×10^{-9}
1.50 g	-0.81	2.00×10^{-7}

Table S4 EIS fitting data of waterborne epoxy resin coating doped with multi-interface structured zinc phosphate particles (Epoxy@ZPNF) with different concentrations.

Sample	0.25 g	0.50 g	1.00 g	1.50 g
CPE_c ($ohm^{-1}\cdot cm^{-2}\cdot s^n$)	7.899×10^{-11}	7.674×10^{-12}	7.564×10^{-13}	1.529×10^{-11}
n_c	0.6955	0.8743	1	0.8071
R_c ($ohm\cdot cm^2$)	2.033×10^{5}	2.763×10^{6}	2.161×10^{7}	1.611×10^{6}
CPE_{dl} ($ohm^{-1}\cdot cm^{-2}\cdot s^n$)	3.853×10^{-10}	1.591×10^{-11}	2.146×10^{-13}	1.215×10^{-10}
n_{dl}	0.9236	0.8044	0.7216	0.8002
R_{ct} ($ohm\cdot cm^2$)	1.862×10^{5}	2.117×10^{6}	1.433×10^{7}	1.191×10^{6}
χ	1.1×10^{-4}	1.5×10^{-3}	3.2×10^{-3}	1.4×10^{-3}

Table S5 Corrosion potentials and corrosion current densities of waterborne epoxy resin coating doped with multi-interface structured zinc phosphate particles (Epoxy@ZPNF) with different thicknesses.

Sample	E_{corr} (V)	i_{corr} ($A\cdot cm^{-2}$)
100 μm	-0.74	6.31×10^{-9}
200 μm	-0.76	8.13×10^{-9}
300 μm	-0.73	3.98×10^{-9}
400 μm	-0.72	6.31×10^{-9}

Table S6 EIS fitting data of waterborne epoxy resin coating doped with multi-interface structured zinc phosphate particles (Epoxy@ZPNF) with different thicknesses.

Sample	100 μm	200 μm	300 μm	400 μm
CPE_c ($ohm^{-1}\cdot cm^{-2}\cdot s^n$)	4.704×10^{-12}	1.546×10^{-12}	7.564×10^{-13}	9.133×10^{-13}

n_c	0.9432	0.9766	1	0.9874
R_c (ohm·cm^2)	1.006×10^{7}	1.233×10^{7}	2.161×10^{7}	1.927×10^{7}
CPE_{dl} (ohm^{-1}·cm^{-2}·s^n)	9.452×10^{-13}	6.015×10^{-13}	2.146×10^{-13}	5.046×10^{-13}
n_{dl}	0.6999	0.7078	0.7216	0.7134
R_{ct} (ohm·cm^2)	1.148×10^{7}	1.255×10^{7}	1.433×10^{7}	1.302×10^{7}
χ	2.3×10^{-4}	2.8×10^{-3}	3.2×10^{-3}	4.1×10^{-3}